Methods and Applications in Fluorescence

RECEIVED
9 February 2018

REVISED
9 November 2018

ACCEPTED FOR PUBLICATION
7 December 2018

PUBLISHED
24 January 2019

TOPICAL REVIEW

Sensing with photoluminescent semiconductor quantum dots

Margaret Chern[1], **Joshua C Kays**[2], **Shashi Bhuckory**[2] **and Allison M Dennis**[1,2]

[1] Department of Materials Science and Engineering, Boston University, Boston, United States of America
[2] Department of Biomedical Engineering, Boston University, Boston, United States of America

E-mail: aldennis@bu.edu

Keywords: ELISA, FLISA, FRET, intrinsic sensor, biosensing, fluorescent sensor, ratiometric sensor

Abstract

Fluorescent sensors benefit from high signal-to-noise and multiple measurement modalities, enabling a multitude of applications and flexibility of design. Semiconductor nanocrystal quantum dots (QDs) are excellent fluorophores for sensors because of their extraordinary optical properties. They have high thermal and photochemical stability compared to organic dyes or fluorescent proteins and are extremely bright due to their large molar cross-sections. In contrast to organic dyes, QD emission profiles are symmetric, with relatively narrow bandwidths. In addition, the size tunability of their emission color, which is a result of quantum confinement, make QDs exceptional emitters with high color purity from the ultra-violet to near infrared wavelength range. The role of QDs in sensors ranges from simple fluorescent tags, as used in immunoassays, to intrinsic sensors that utilize the inherent photophysical response of QDs to fluctuations in temperature, electric field, or ion concentration. In more complex configurations, QDs and biomolecular recognition moieties like antibodies are combined with a third component to modulate the optical signal via energy transfer. QDs can act as donors, acceptors, or both in energy transfer-based sensors using Förster resonance energy transfer (FRET), nanometal surface energy transfer (NSET), or charge or electron transfer. The changes in both spectral response and photoluminescent lifetimes have been successfully harnessed to produce sensitive sensors and multiplexed devices. While technical challenges related to biofunctionalization and the high cost of laboratory-grade fluorimeters have thus far prevented broad implementation of QD-based sensing in clinical or commercial settings, improvements in bioconjugation methods and detection schemes, including using simple consumer devices like cell phone cameras, are lowering the barrier to broad use of more sensitive QD-based devices.

1. Introduction

Fluorescence is a powerful tool for imaging and detection. Its superior signal-to-noise (S/N) compared to other optical techniques and the multiple photophysical measurement approaches lend it to numerous applications, including sensing. Photon energy (*i.e.*, wavelength/color), photoluminescence (PL) intensity, and PL lifetime can all be modified and thus harnessed as sensor outputs [1]. Numerous fluorophores including organic dyes, fluorescent proteins, and lanthanide-based emitters have been coupled to signal transduction elements to produce fluorescent sensors [2], but in this review, we specifically discuss the role of semiconductor quantum dots (QDs) in the field. Photophysically, the simplest QD-based sensors use the unmodulated emission of QDs as an indication of whether or not a QD-tagged moiety is present, such as when fluorescence aids visualization [3] or indicates the binding of a QD-labeled biomolecule [4–7]. Alternatively, intrinsic photophysical mechanisms can be harnessed to tie specific environmental factors such as temperature to calibrated changes in the QD emissive properties. In this way, the QD itself becomes both the sensor and transduction element and changes in the environment are quantified through changes in PL intensity, wavelength, or lifetime [8–20]. Using additional quenchers or fluorophores to modulate QD photophysics in energy transfer schemes adds another layer of complexity to the sensors that enables specific detection of analytes through molecular recognition elements [21–31]. The nanoparticle structure of QD-based sensors facilitates the integration of multiple sensing and modulating

© 2019 IOP Publishing Ltd

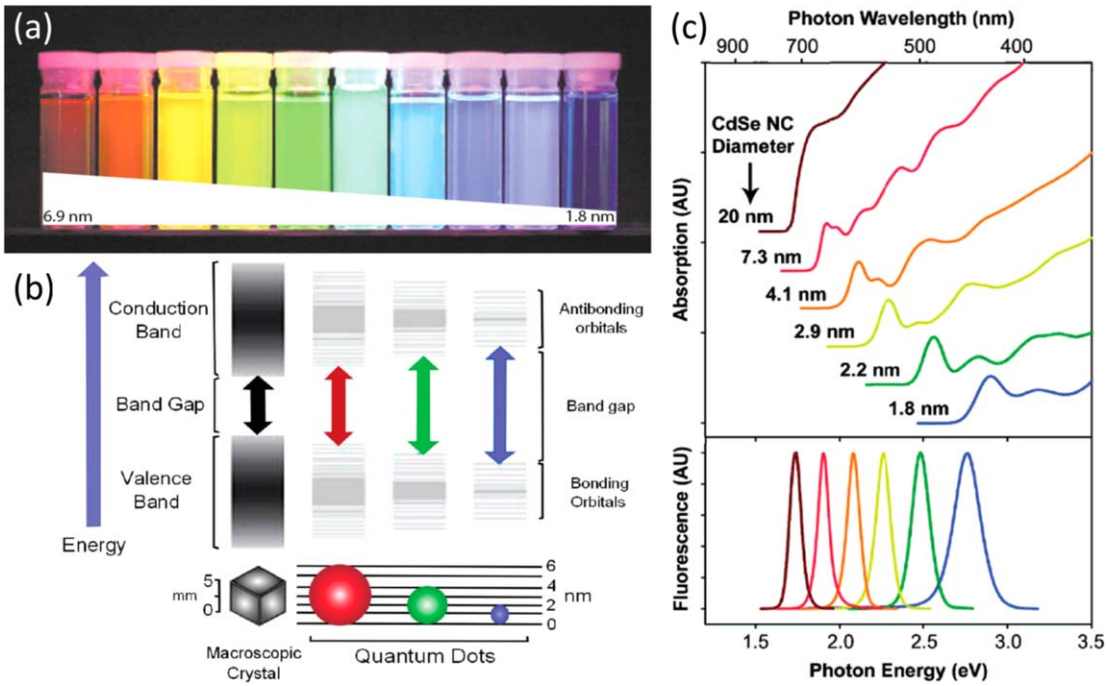

Figure 1. (**a**) Quantum dots of different sizes emitting at colors across the visible wavelength range. (**b**) A diagram showing quantization of energy levels in semiconductor crystals as they decrease in size on the nanoscale. (**c, top**) Absorption and (**c, bottom**) emission spectra of CdSe QDs of different sizes. QDs exhibit broadband absorption above their bandgap and exhibit symmetric emission profiles. Reprinted from [41]. Distributed under a Creative Commons Attribution Non-Commercial License 4.0 (CC BY-NC).

elements [32, 33], allowing for complex or multiplexed signaling [24, 28, 34–37]. In this review, we discuss the underlying photophysics supporting the various sensor types as well as examples that demonstrate applications of each method.

2. Quantum dot fundamentals

Quantum dots (QDs) are semiconductor nanocrystals exhibiting fluorescent properties due to quantum confinement. Quantum confinement occurs when a material is reduced to a size similar to the characteristic length of the property being probed [38]. For QDs, this characteristic length is the exciton Bohr radius (the distance between the electron-hole pair), thus QDs on the same size scale as their material's characteristic exciton Bohr radius exhibit quantum confinement [39, 40]. QD fluorescence originates from the recombination of an electron-hole pair, and fluorescence is initiated by the photoexcitation of an electron from the QD valence band into its conduction band. The electron relaxes to the lowest energy level in the conduction band before recombining with the hole left behind in the valence band. The difference in energy between the conduction and valence band is conserved in the form of an emitted photon, thus, the size of this gap dictates the energy/wavelength of the light emitted from the QD (figure 1) [38, 41, 42]. The QD bandgap is directly related to its diameter, and therefore QDs comprising the same semiconductor material can be tuned to emit different wavelengths by simply changing their size. More recently, QDs made of different types of materials have been synthesized, such as graphene [43] and silicon [44], but this review will focus specifically on direct bandgap semiconductor QDs.

3. Quantum dots as indicator dyes in sensors

An advantage of QDs compared to other fluorophores is their large absorption cross-section. Brightness is determined by the amount of light a molecule can absorb (molar extinction coefficient, ε) and the efficiency with which the absorbed energy is converted into emitted light (quantum yield, QY) [45]. While both organic fluorophores and QDs may exhibit near unity QYs, the absorption cross-section of QDs may be orders of magnitude higher [46]. Heterostructured core/shell QDs provide further opportunity to tailor the absorption cross-sections of QDs leading to brightness-matched multicolor QDs and brightness-enhanced thick-shelled QDs [25, 47]. The brightness of QDs make them an effective choice when picking fluorescent labels to tag objects. For example, nanopipettes used for taking voltage recordings of dendritic spines have been coated with QDs to enable clear visualization of the pipettes for precise placement on cell structures (figure 2) [3]. While QDs were not the focus of the scientific questions being studied, they were used effectively as a tool to facilitate experimental methods.

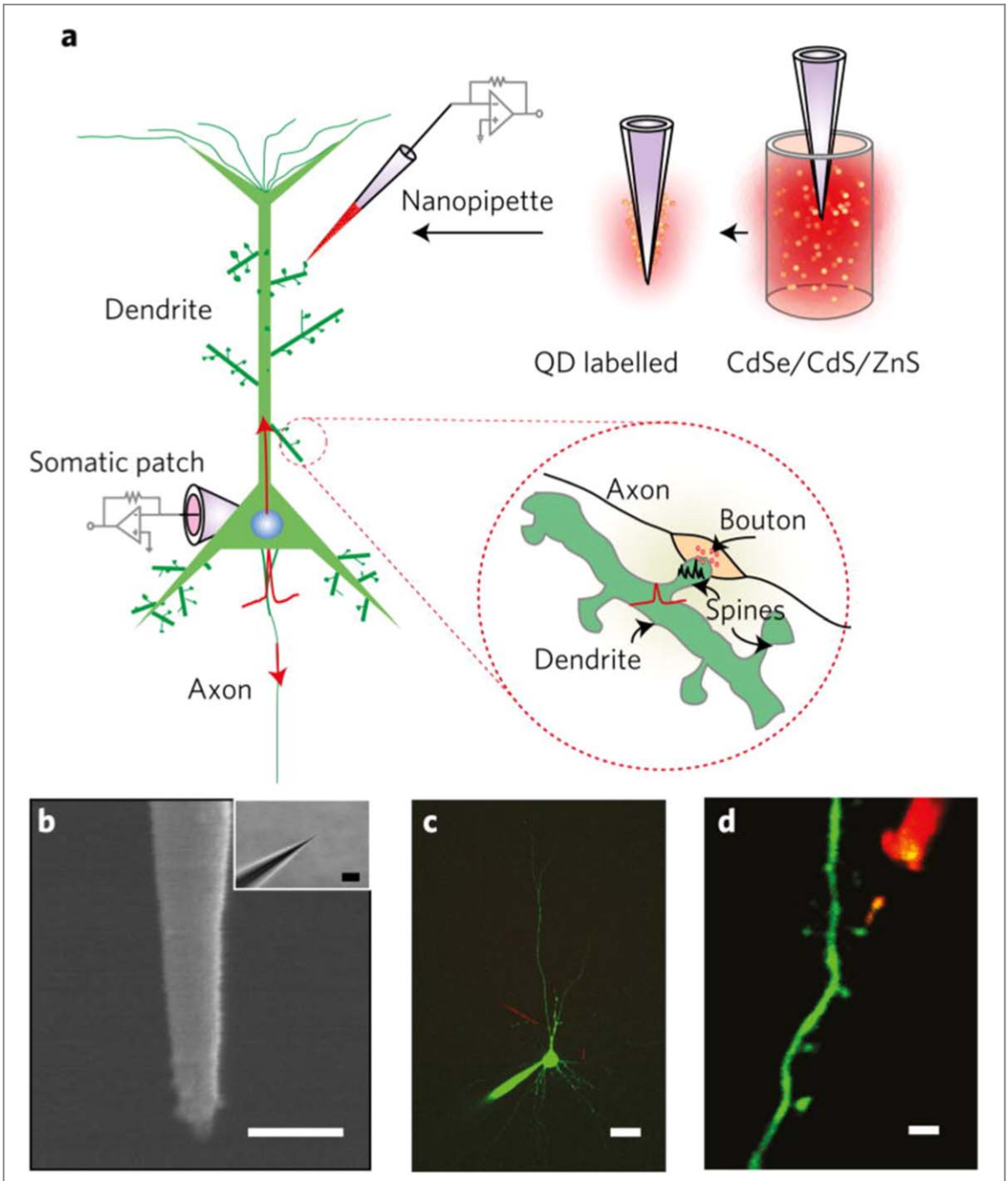

Figure 2. QD-coated nanopipettes used for taking voltage recordings of dendritic spines. Coating the nanopipettes with red QDs allowed for precise placement of the nanopipette. Reprinted with permission from [3]. Copyright 2016 Springer Nature.

As in the nanopipette example, QDs incorporated into existing visualization schemes as alternatives to organic dyes or fluorescent proteins are effective indicators in sensing platforms. QDs have generated interest as alternative fluorescent labels due to their excellent chemical- and photo-stability, narrow bandwidths, exceptional brightness, and large surface area available for surface functionalization [33, 46, 48]. In sensors, the binding or unbinding of a species is monitored by fluorescently labeling one or more of the parts involved in the interaction. Binding/unbinding changes the concentration of the fluorophore in the visualized region, resulting in a change in fluorescence intensity. A common, widely used sensing format based on this scheme is the enzyme-linked immunosorbent assay (ELISA). ELISAs use antibody binding to detect a target antigen or antibody with enzyme catalyzed colorimetric reactions used to indicate the presence of the bound antibody. Assays that utilize a fluorescent label instead eliminate the incubation time necessary to develop the color and are called fluoroimmunoassays or FLISAs. Generally, fluorescence assays have higher signal to noise ratios than colorimetric assays, resulting in lower limits of detection (LOD) [49]. For example, ThermoFisher Scientific sells a broad range of immunosorbent assay products

using both colorimetric and fluorescent detection methods. Currently, the lowest detectable concentration for a colorimetric product is 20 pg mL^{-1} (Ultra TMB, 34028) while all fluorescence based ELISAs have LODs < 5 pg mL^{-1}, with the lower limit of the QuantaRed Enhanced Chemifluorescent Substrate assay reaching 4 pg mL^{-1} [50].

An advantage of using QDs instead of dyes or catalysts is the availability of their relatively large nanoparticle surface for a variety of functionalization schemes. Self-assembly mechanisms can be used to bind biomolecules to the metal ion surface of the QD, making for flexible and relatively simple labeling. Perhaps one of the first examples of self-assembled antibody/QD conjugates (Ab-QDs) and their use in a FLISA was shown by Goldman *et al* [51]. In their design, antibodies were engineered to include positively charged leucine zippers for electrostatic interaction driven self-assembly to QDs coated with the negatively charged small molecule ligand dihydrolipoic acid (DHLA). Shortly after their publication, histidine self-assembly to the QD metal ion surface was reported [52]; since the antibodies used in the Goldman report utilized histidine domains to facilitate protein purification, the exact mechanism of binding to the QD surface is unclear. Nevertheless, the utility of the Ab-QDs was demonstrated in both direct and sandwich fluorometric assays of Staphylococcal enterotoxin B (SEB) as well as in plate-based and flow-displacement formats for TNT sensing. While direct comparison to commercially available FLISAs/ELISAs was not performed, the feasibility of the QD-FLISA system was successfully demonstrated [51].

Compared to colorimetric ELISAs or organic dye-based FLISAs, QDs present tremendous multiplexing potential. Due to their broadband absorption in the UV, multiple QDs emitting at distinct wavelengths can be excited with a single excitation wavelength. In 2009, Peng *et al* created an assay incorporating five distinct QD emitters per well for simultaneous detection of substances often illegally used on food animals in China: dexamethasone, gentamicin, clonazepam, medroxyprogesterone, and ceftiofur [7]. Each of the QDs were functionalized through self-assembly with biotinylated, denatured BSA before further functionalization with an avidin-labeled antibody. While the binding capacity of the Abs was significantly reduced when attached to QDs, the FLISA was still used to detect each species in relevant concentration ranges with less than 0.1% cross-reactivity between the chemically distinct analytes. Following drug administration, animal tissue was harvested and homogenized after 1, 2, 3 and 7 days. Liquid sample extracts were tested with the FLISA and the values quantified were within reasonable agreement for dexamethasone and within a standard deviation for medroxyprogesterone acetate compared to the results from a traditional ELISA.

Using the antibody binding scheme presented by Peng *et al* [7], Zhu *et al* developed a multiplexed hybrid assay using both commercial QDs and horse radish peroxidase (HRP) for sensing [6]. This hybrid immunoassay was used for simultaneous detection of quinolone and sulfonamides in milk samples. The design incorporated both direct and indirect binding, along with both fluorescence and colorimetric based sensing in a single well. Another multi-color QD-FLISA reported by Song *et al* in 2015 detected the residues of multiple antibiotics in milk. Their competitive fluorescence immunoassay consisted of antibodies that bound to the well plate in the absence of the antibiotics of interest. Rather than mixing all antibiotic-antibody pairs into a single well, a fluorescence imaging array was used to simultaneously measure 96 wells at once. Specific responses to each antibiotic were observed in milk samples with good sensitivity and accuracy when compared to results of the same samples tested with traditional ELISAs. The authors noted that in addition to quantitative fluorescent measurements, semi-quantitative information could be obtained from visual inspection and a standard color chart. The demonstration of these color charts (figure 3) show potential for translation of the sensor to a detection system for daily food safety control [53]. Because the different antibody-antibiotic pairs were never mixed in the same well, different QD colors were not actually necessary. However, since all of the QDs could be excited at the same wavelength, the incorporation of multiple colors eases visual inspection with no extra measurement steps, something that would not be possible when using traditional fluorophores with smaller Stokes shifts. More recently, a FLISA was developed for detection of C-reactive protein (CRP) [4], a critical biomarker for cardiac infarct. CdSe/ZnS QDs coated with an amphiphilic polymer, polymaleic acid n-hexadecanolester (PMAH), and covalently labeled with antibodies through carbodiimide crosslinker chemistry were used as labels. Clinical samples were collected and used in both the developed FLISA and the gold standard Roche immunoturbidimetry assay. The FLISA showed excellent accuracy. Immunoturbidimetry is a method of protein quantification that relies on the formation of antigen-antibody complexes that precipitate from solution; the turbidity of the solution is measured to quantify protein content. Immunoturbidimetry is fast and sensitive, but requires expensive instrumentation; ELISAs are economical by comparison, but often take longer than an hour to develop [54]. The total time required for the FLISAs was 50 min, shorter than a typical ELISA assay, showing potential for development into a rapid and cost-effective diagnostic tool [4].

Plate-based ELISAs have been standard in clinical labs for over 20 years [55], but their assay protocols involve several washing and incubation steps that require time and expertise. The advantage, however, is precise quantification of the analyte of interest. In

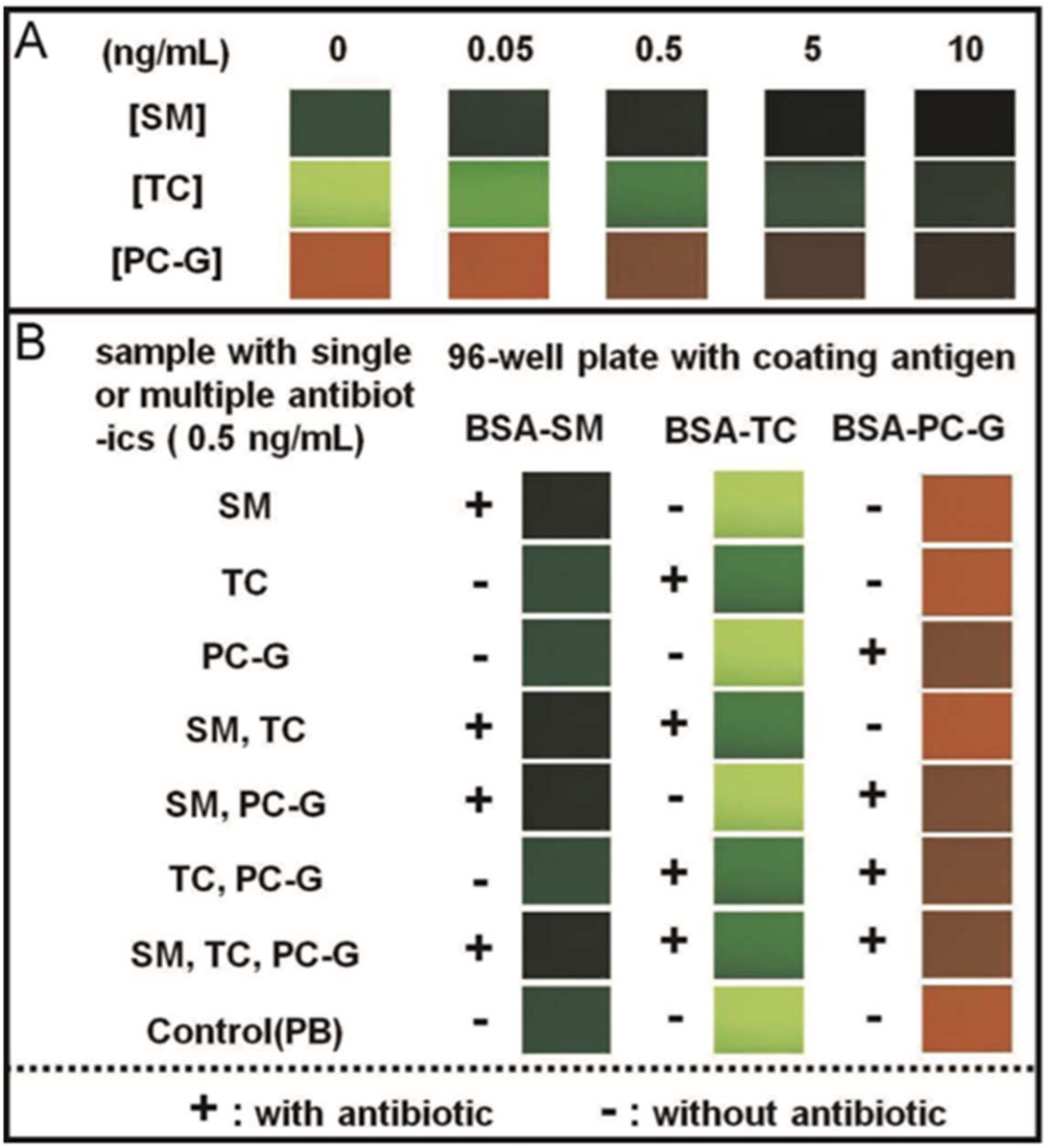

Figure 3. A color chart for visual, qualitative determination of streptomycin (SM), tetracycline hydrochloride (TC), and penicillin G (PC-G) concentrations in milk. Panel (**a**) provides a color-key for comparison to the colors collected from real samples in panel (**b**). All wells with antibiotics show a visual change in color from their non-antibiotic controls. Figure reprinted with permission from [53]. Copyright 2015 Elsevier.

some cases, precise quantification is not needed, and testing for relevant clinical thresholds for disease is enough to yield a yes-no diagnosis. In these cases, point-of-care (POC) devices can be particularly useful. POCs devices are meant for diagnostic screening at or near the patient site of care. To be effective, they must be affordable, reliable, and user friendly [56].

Lateral flow assays (LFAs) are well established as POC devices. LFAs are paper strip sensors that require very little sample and no washing steps. They consist of a sample pad, a conjugate pad, a membrane, and an absorbent pad. The liquid analyte is applied to the sample pad and flows towards the absorbent pad via capillary action. In the presence of the analyte of interest, the conjugate reporter binds to capture strips along the pad, indicating whether the sample is positive or negative for the analyte in question. Traditionally, LFAs use colloidal gold or latex particles. By using quantum dots as a fluorescent readout, the sensitivity of existing LFAs is improved [49]. Several QD based FLAs have been demonstrated for the detection of different viruses [57, 58], biomarkers [4, 59–62], and food contaminants [49, 63].

In 2016, Wu *et al* developed a QD FLISA-based flow strip assay for detection of 2 influenza subtypes, H5 and H9 (figure 4). Assay strips were fabricated by painting stripes of the H5 and H9 antibodies as well as a control IgG antibody onto commercially available nitrocellulose membrane. 147 samples collected by the Shenzhen Entry–Exit Inspection and Quarantine Bureau were tested with both the FLISA and real-time polymerase chain reaction (rt-PCR) as a

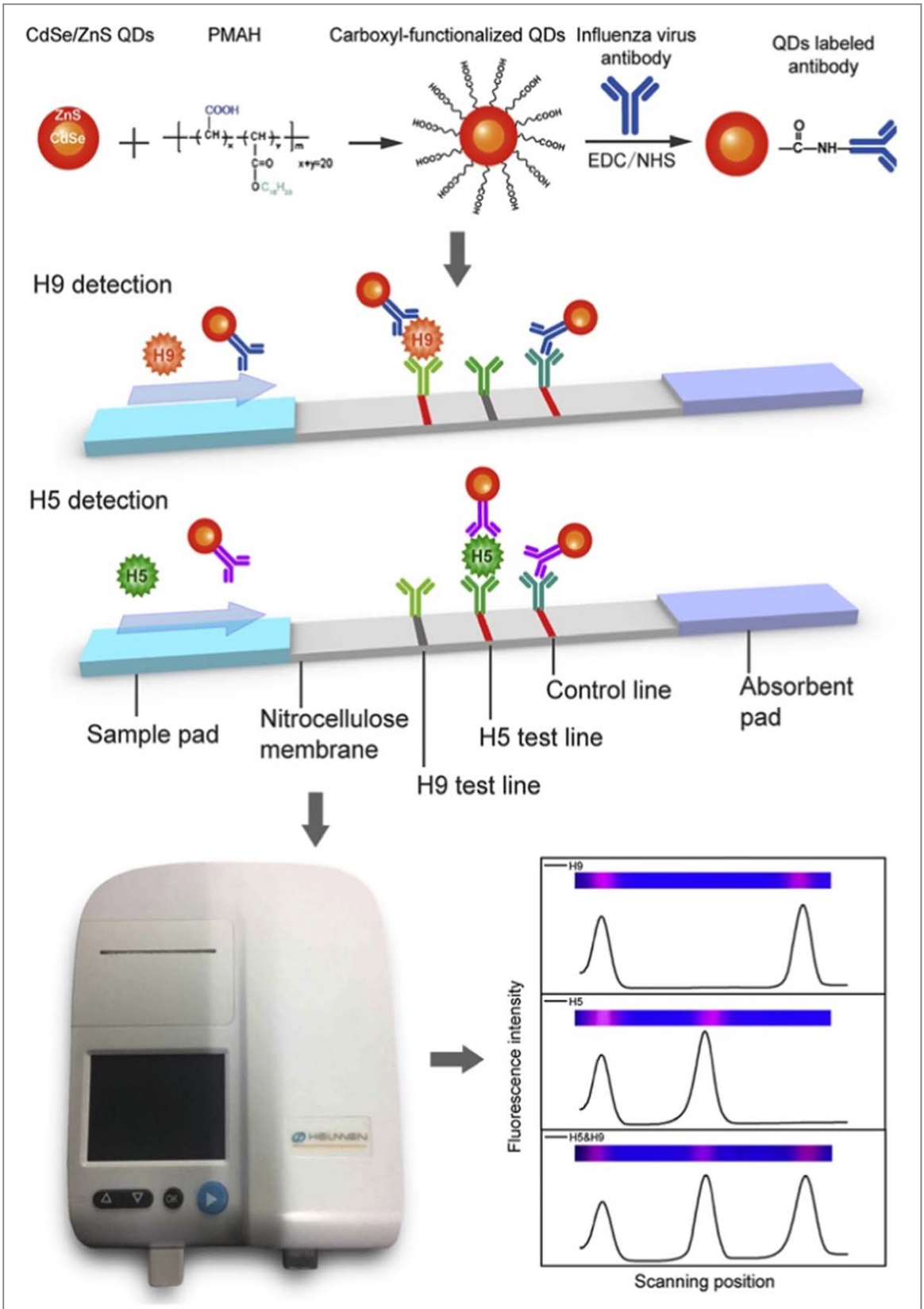

Figure 4. Schematic of a flowstrip-based QD-FLISA for H5N1 and H9N2. CdSe/ZnS QDs functionalized with the polymer PMAH are labeled with antibodies for either H5 or H9 and allowed to travel across the nitrocellulose membrane. In the presence of H9 or H5, the Ab-QDs form a sandwich complex with their respective antibodies dried onto the test strip. QDs not bound by H5N1 or H9N2 are captured on the control line (IgG). Because test lines for each influenza subtype are spatially separated, only 1 QD color needs to be used. The LFA can be read visually or in an instrument for improved LODs. Reprinted with permission from [58]. Copyright 2015 Elsevier.

reference. Rather than employing a conjugate pad on the strip, each sample was pre-mixed with the H9 and H5 Ab-QDs before loading onto the sample pad. The results from the two assays matched 100%, verifying the accuracy of the QD-FLISA. While real-time PCR can take several hours, the flow strip assay could be

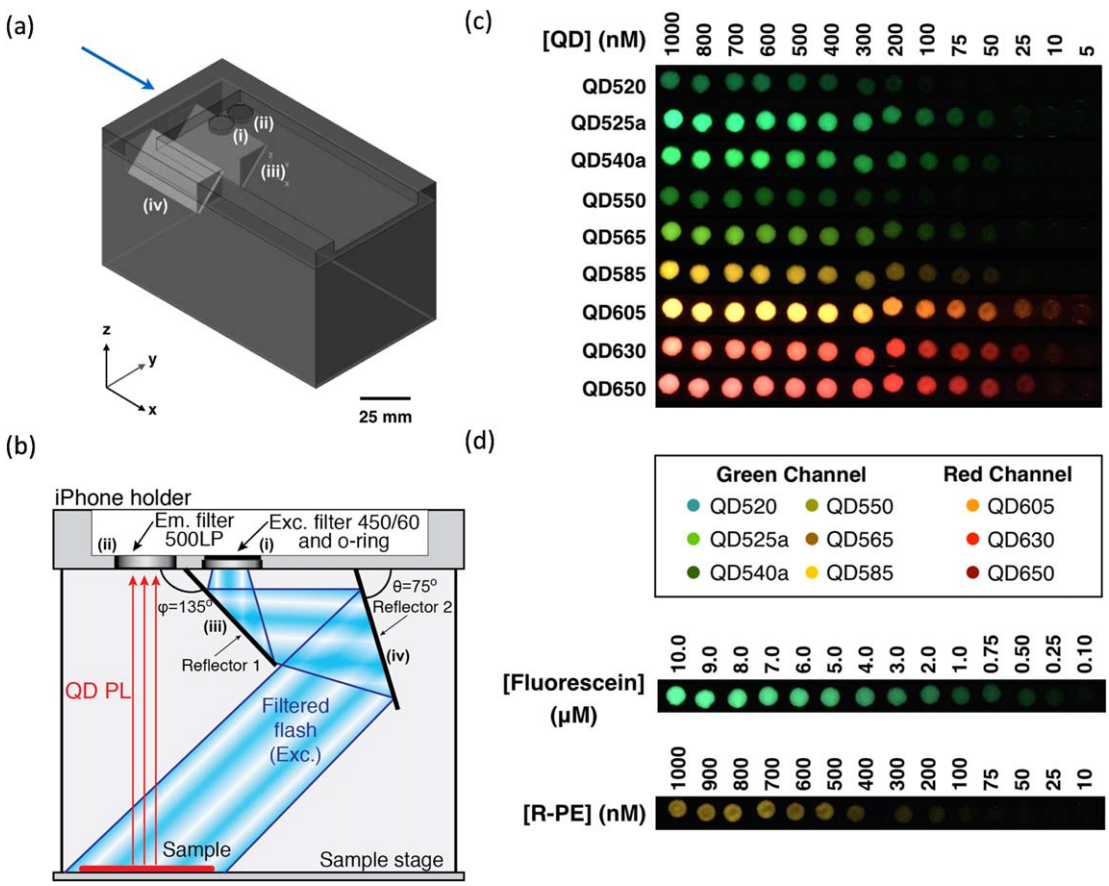

Figure 5. (**a**) CAD drawing of a 3D-printed holder and (**b**) schematic of the internal functionality of the smartphone fluorescence imager. (**c**) Images of different QD emitters at different concentrations (4 nM–1 μM) compared to (**d**) fluorescein (100 nM–10 μM) and R-PE (10 nM–1 μM). Adapted with permission from [68]. Copyright 2016 Springer Nature.

read out 15 min after the sample was applied, greatly shortening the time between sample collection and result [58]. For point-of-care diagnostics, it is important that the time to sensor output fits within a reasonable clinical appointment time to ensure that any relevant diagnoses are relayed to the patient before they leave the clinic to facilitate appropriate and timely treatment [64].

The cost of a diagnostic is determined by the cost of consumables per assay, time per assay, and the instruments needed to analyze the assay. While fluorescent readouts can increase assay sensitivity, the tradeoff is the cost of requisite equipment needed to measure fluorescence. The quality of a fluorimeter greatly influences its price, but even the simplest fluorimeters are benchtop instruments. The development of compact, mobile, and economical devices for measuring fluorescence would greatly advance QD based diagnostics, especially for POC formats. To this end, a recent push for developing ways to take fluorescent measurements with readily available consumer devices such as cell phones has been seen in the field [55, 64–68].

For example, in 2016 Petryayeva and Algar demonstrated the feasibility of using a smartphone, 3D printed holder, two optical filters, and low-cost plastic reflectors for imaging QDs on a variety of substrates [68]. A test streptavidin-biotin binding assay as well as a Förster Resonance Energy Transfer (FRET)-based proteolytic assay showed the feasibility of using smartphones as an application-based fluorescence imaging tool. Additionally, a comparison to the commonly used dyes fluorescein and R-phycoerythrin (R-PE) showed that the detectable concentration of QDs were approximately an order of magnitude lower. In this comparison, the brightness mismatch between differently colored QDs also became apparent, indicating the need to create brightness matched QDs across different emission wavelengths (figure 5). Nonetheless, this report nicely highlighted the advantage of using bright and photostable QDs when developing cheap imaging platforms based on readily accessible consumer devices.

4. Quantum dots as intrinsic sensors

In the sensors previously discussed, the sensing mechanism is external to the QD. In this section, the sensors utilize changes in fluorescence due to properties characteristic to the QDs themselves.

4.1. Using QD photophysics for thermometry

Regardless of material type, fluorescent emitters exhibit temperature-dependent fluctuations in their emission intensity [45, 69]. Fluorescent particles absorb light as energy and dissipate that energy radiatively as emitted light, or non-radiatively through various other pathways. The rate of non-radiative transitions, k_{nrt}, is dependent on temperature following the Arrhenius equation [45, 69]:

$$k_{nrt} \sim e^{\frac{E}{kT}} \quad (1)$$

where ΔE is the size of the energy gap between the lowest level excited state and non-radiative decay state and k is the Boltzmann constant. If the rate of non-radiative transitions increases, the efficiency of light conversion decreases, resulting in a decrease in emission intensity. In addition to PL intensity, the emission profile with respect to wavelength can also change as a function of temperature. Semiconductor bandgaps, E_g, are temperature dependent and can be loosely described by the Varshni relation [70],

$$E_g(T) = E_0 - \alpha T^2/(T + \beta) \quad (2)$$

where E_0 is the semiconductor's inherent bandgap, T is temperature and α and β are fitting parameters characteristic to the semiconductor. Just as in bulk semiconductors, QD bandgaps, and therefore their PL energy/wavelength, are affected by temperature. Several different core, core/shell, and alloyed QD structures have been studied for fluorescence temperature dependence including CdSe [71, 72], CdTe [73], ZnSe/ZnS [74], CdHgTe [75], InGaN [76], HgTe [77], and alloyed core CdSeZnS/ZnS[78] QDs. Other factors that can impact how temperature affects emission include the presence of dopants [79, 80], different surface ligands [81, 82], and the surrounding environment/matrix [79, 83].

As early as 1996, Dieguéz *et al* [79] used photoreflectance studies to show that the Varshni relation is valid for CdTe nanocrystals for the entire temperature range tested (14–400 K). By measuring the temperature-dependent PL of three different sizes of CdTe QDs, Morello *et al* [73] examined not only how the quantum confinement-based bandgap changes as a function of temperature, but also changes in the QD fluorescence intensity. Each of the QDs exhibited a decrease in fluorescence intensity, increase in the full width at half maximum (FWHM) of the emission peak, and red-shift in peak PL wavelength with increased temperature. Their results were categorized in two temperature regimes: <170 K and >170 K. At low temperatures, PL quenching was attributed to a transition between intrinsic energy states and defect states. At temperatures above 170 K, thermal escape, a process mediated by exciton-optical phonon interactions, was observed. The amount of PL quenching was highly dependent on QD size, with larger QDs exhibiting increased exciton-phonon coupling. In 2005, Valerini *et al* showed that the change in PL emission wavelength is due to exciton-phonon coupling rather than confinement energy of the exciton [84]. The change in the QD bandgap of CdSe and CdSe/ZnS QD immobilized in polystyrene (PS) was fitted to the Varshni relation and the values for α and β were found to be in range of previously reported values for bulk CdSe. The similarity of temperature dependence to bulk CdSe indicated that QD confinement potentials are independent of temperature, but that exciton-phonon coupling is strongly affected by quantum confinement.

In addition to size, the QD structure and the presence or absence of dopants can impact the temperature dependence of the photoluminescence. A study comparing core only CdTe QDs and core/shell CdTe/CdSe QDs of different CdSe thicknesses [85] showed that temperature-dependent PL quenching was enhanced as the CdSe shell thickness increased. This was attributed to the increased Type II nature of the QDs with increased shell size. In a Type II QD heterostructure, the electron and hole are spatially separated, decreasing the Coulomb interaction between them. This results in a lower activation energy for exciton decomposition, increasing the effect of temperature on PL intensity. Surprisingly, the typical red-shift in PL was not observed for the Type II CdTe/CdSe QDs. The authors speculated that the core/shell interface experiences atomic interdiffusion at high temperature, which could result in a blue-shift in the PL emission. They argued that in their system, the two effects may have canceled each other out. PL measurements with temperature hysteresis curves were not generated for their study, so the validity of this explanation is unclear. The effect of lattice strain due to the difference in lattice parameters of CdTe and CdSe is also discussed, but does not explain the behavior seen in their study, as CdSe/ZnS QDs, which also have high lattice strain, exhibit temperature-dependent PL wavelength shifts [84]. As early as 1996, Pal *et al* [79] showed that bandgap temperature dependence on germanium-doped CdTe QDs is well described by the Varshni equation, while this is not the case for vandium-doped CdTe QDs. More recently, Harbord *et al* [80] reported that the radiative lifetime of undoped InAs/GaAs increased by 3 ns between 12 and 300 K, whereas this increase was suppressed by a factor of two by p-doping the structure.

In contrast to the previously discussed papers, Reznitsky *et al* [86] explored how temperature dependence is impacted by excitation power in a study of five epitaxially grown CdTe/ZnTe quantum wells (QWs) grown with various CdTe thickness separated by 60 nm-thick ZnTe barriers. Samples exposed to lower excitation density (1 W cm^{-2}) were much more susceptible to losses in PL intensity at higher temperatures compared to samples exposed to higher excitation density (100 W cm^{-2}). The effect was lessened as the size of the CdTe layer increased due to the increase in non-radiative pathways for the less well confined structures. PL quenching occurs with an increase in

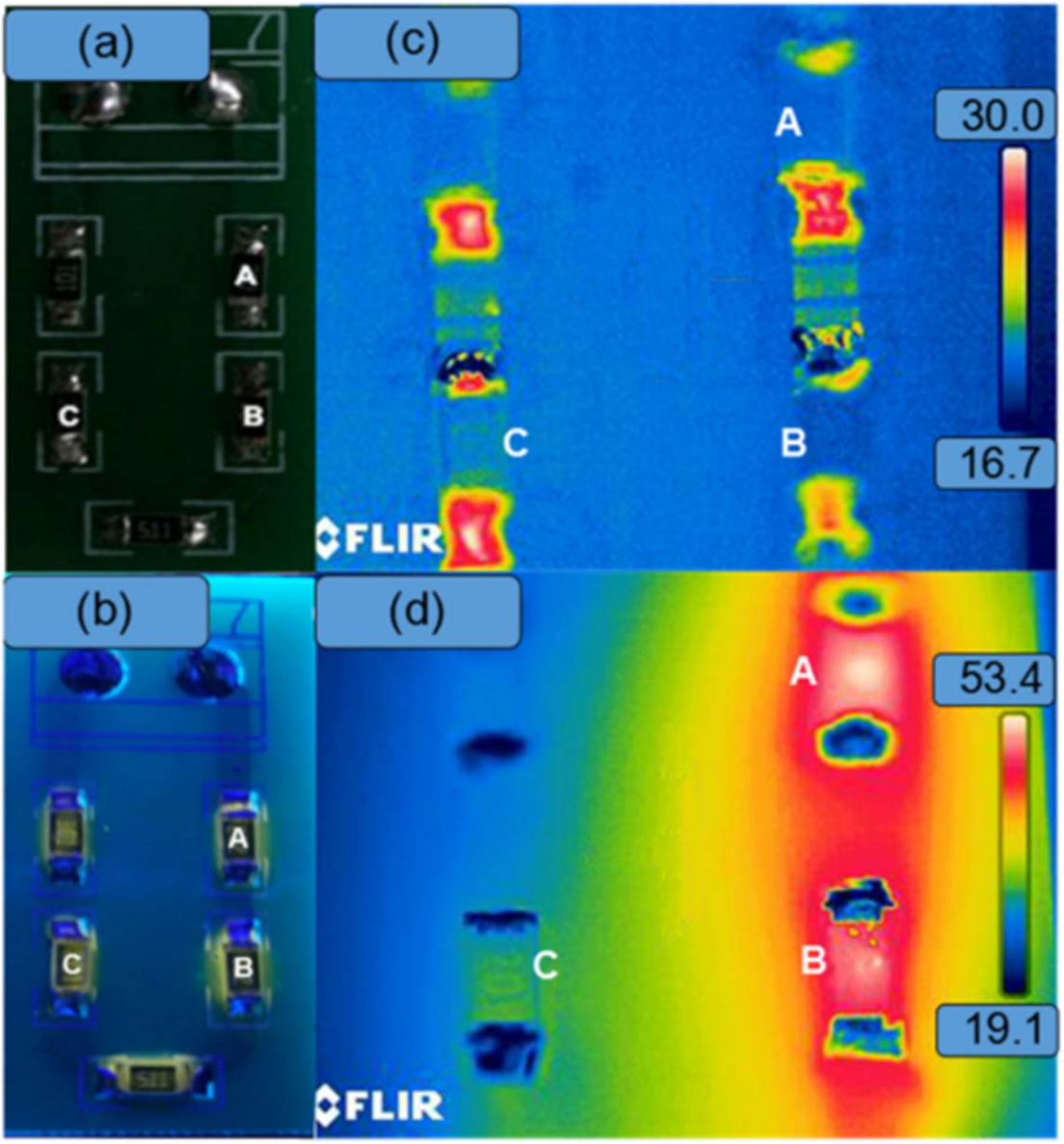

Figure 6. A circuit (**a**) without and (**b**) with dropcast QD film under UV illumination. (**c**) Thermal infrared images of the circuits operating at 0 mA and (**d**) 7.9 mA. Resistors A, B, and C had resistances of 1982 Ω, 992 Ω and 196 Ω, respectively, resulting in different local surface temperatures during circuit operation. The color scales are in units of °C. Reprinted with permission from [12]. Copyright 2014 Institute of Physics.

the rate of non-radiative relaxation (equation (1)); the authors assert that by exciting at a higher power density, more of these pathways are saturated, resulting in decreased temperature dependence. Although the explanation is satisfying, PL lifetime measurements were not reported to verify this mechanism. While this report was quite short, and the temperature dependence was described simply as 'complicated,' the qualitative observation of power dependence is of interest for sensor device design. These results are a reminder that careful experimental design and calibration is necessary to ensure that observations of changes in PL intensity, lifetime, or wavelength are due to the parameter being measured, like temperature, and not confounding factors such as a change in QD concentration or excitation power. Follow-up studies using colloidal QDs would help to elucidate the effect of excitation power on PL temperature dependence.

The temperature-dependent PL properties of QDs naturally lend them to optical temperature sensing. Optical sensors are advantageous for temperature sensing with high spatial resolution without requiring an invasive temperature probe [8, 9, 12]. Methods of incorporating QDs into devices as temperature sensors range from simple to rather complicated, depending on the application. In a simple case, commercially available CdS_xSe_{1-x}/ZnS QDs dispersed in toluene were mixed with VGE-7021 varnish to produce a paint that could be applied easily to surfaces [10]. This QD paint was used for real time temperature sensing during magic-angle spinning nuclear magnetic resonance (MAS NMR) measurements.

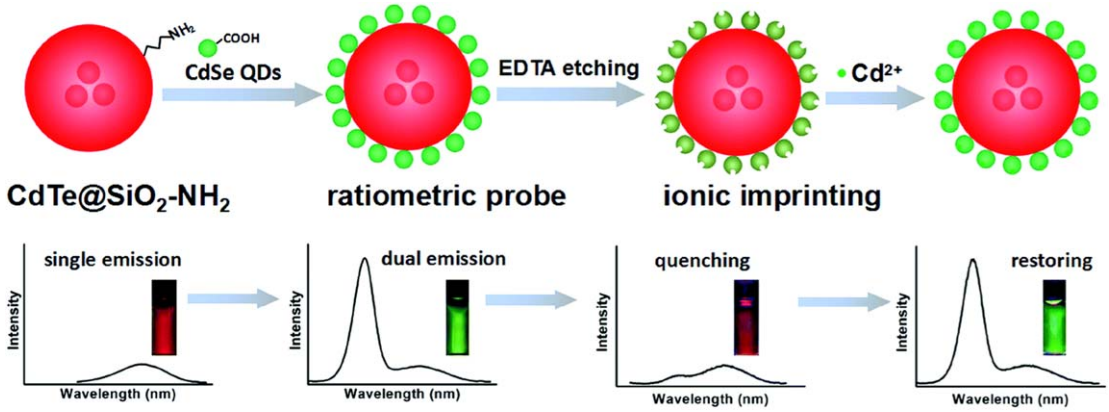

Figure 7. CdTe QDs emitting red are encapsulated in large silica nanoparticles which are then surface labelled with green emitting QDs. EDTA is used to etch the green QDs of their surface Cd^{2+} ions, resulting in quenching of green emission and overall red emission of the probe. The addition of Cd^{2+} ions fills the etched surfaces of the green QDs, resulting in a re-brightening of the surface QDs and change of the overall probe emission from red to green. Here, the red emission does not change because it is protected inside the silica nanoparticle and is used as a calibrator for the sensor as a whole. Reprinted with permission from [16]. Copyright 2016, Royal Society of Chemistry.

The outer surface of the MAS rotor was coated with the QD paint and a simple optical fiber was rigged for excitation and collection of QD PL. Low temperature NMR has several applications [87–89], but can be challenging due to large temperature gradients within the NMR probe, making it important to monitor the temperature of the sample during measurement for accurate analysis. The QD paint showed a PL peak redshift of 18 nm from 10 K to 323 K and was used to determine the temperature during MAS NMR measurements. Temperature measurements below 50 K were subject to error due to the small change in PL wavelength in that regime. While some methods for determining NMR temperature do exist, the QD paint is external to the sample, eliminating contamination, and can be monitored while NMR measurements are in progress. For temperatures below 50 K, the author noted that perhaps a different composition of QD could be used that is more responsive to temperature in that range.

The idea of embedding a fluorophore in a matrix to create a 'paint' for temperature sensing is not new. In fact, temperature sensitive paints (TSPs) traditionally use small molecule dyes or chemical complexes and are historically used in aerodynamic studies for understanding heat transfer dynamics [90, 91]. A potential benefit of using QDs is their narrow emission bandwidths and broadband UV absorbance profiles. For example, Kameya *et al* used ZnS-$AgInS_2$ nanoparticles (ZAIS) in conjunction with platinum tetrakis (pentafluorophenyl) porphyrin (PtTFPP) for dual temperature and pressure sensing [11]. ZAIS was chosen for the TSP because it could be excited using the same wavelength as PtTFPP while exhibiting negligible emission overlap; this spectral separation would be difficult to achieve in a two-dye system. Matsuda *et al* also examined ZAIS nanoparticles as temperature sensors, touting the additional benefit of their low toxicity [92].

In some cases, the structure to be coated is complex and a more involved strategy for integrating the QDs is needed. For example, Larrión *et al* coated the inner surfaces of the holes of a photonic crystal fiber by means of a layer by layer adsorption technique [93]. Their studies showed that monitoring changes in PL FWHM had a higher average sensitivity than monitoring PL wavelength or intensity. Additionally, it was shown that the sensitivity decreased at lower temperature when looking at PL measurements, while the opposite was true when looking at absorbance measurements. While a discussion of absorbance is not included in the scope of this review, the authors make a good point about combining absorbance and fluorescence recordings to maximize the temperature range in which accurate sensing is possible—an approach that does not require finding a different type of QD with a more sensitive temperature dependence at low T [93].

In 2010, Bensalah *et al* showed that QD PL emission can be used to accurately monitor gold nanoshell (GNS)-mediated temperature changes occurring near cancerous cells following NIR illumination [9]. Photothermal therapy is being developed for cancer treatment [94–96], whereby the illumination of plasmonic structures (typically gold nanoparticles) with NIR light causes localized heating. Using nanoparticles specifically targeted to cancer cells in conjunction with localized NIR illumination may enable selective ablation of cancerous tissue. Imaging QDs in the vicinity of the cells/tissue enables monitoring of the temperature as well as the spatial distribution of the heat—allowing researchers to elucidate appropriate treatment protocols that result in cancer cell death but minimize damage to surrounding cells. For example, in a different study using gold nanostars (GNSts) as a probe for

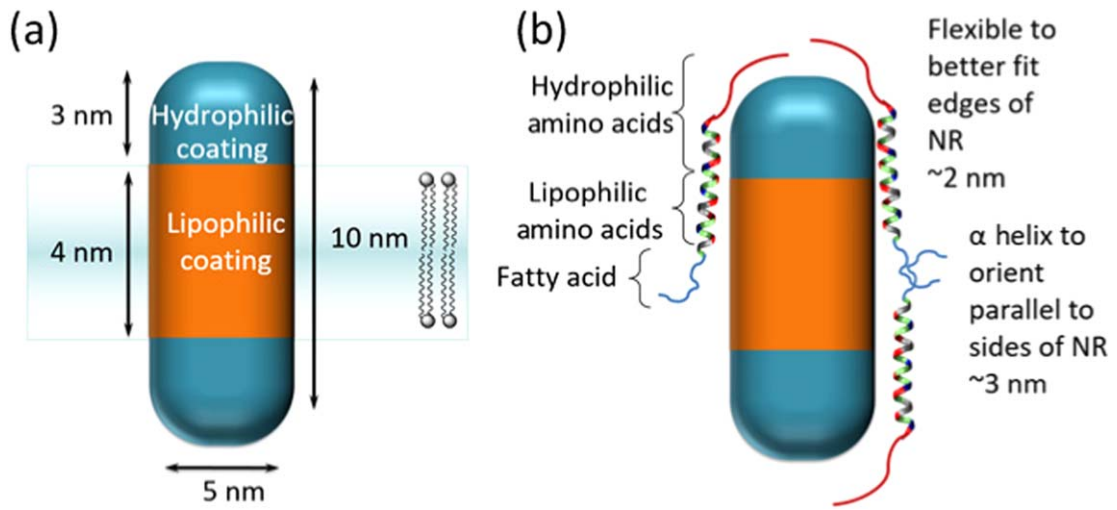

Figure 8. CdSe seeded CdS nanorods (NR) for *in vitro* voltage sensing of cells. Peptides with hydrophobic and hydrophilic regions are used to coat the nanorods in order to align them perpendicularly to the electric field. In the presence of the electric field, the quantum confined Stark effect (QCSE) causes a peak red-shift and reduction in PL intensity. Adapted from [18]. Distributed under a Creative Commons Attribution Non-Commerical License 4.0 (CC BY-NC).

in vivo imaging and photothermal therapy, Liu *et al* [96] characterized heating of the GNSts *in vitro* by monitoring temperature using an infrared (IR) thermal imaging camera. Because calibration of IR thermal imagers can be quite complicated [97], further verification of temperatures using physical probes before and after heating was necessary. Using QD based thermometry may have simplified and improved their *in vivo* temperature measurements. The study by Bensalah *et al* was performed *in vitro,* but recent developments of non-toxic, heavy metal free QDs provide a path towards *in vivo* studies.

In 2014, Liu *et al* used ZnCuInS/ZnSe/ZnS QDs to monitor temperature with spatial resolution on a circuit (figure 6) [12]. The QDs exhibited the same behavior over three rounds of temperature cycling, indicating the reversibility and stability of the QD sensors. This is of particular note, because the use of cadmium-free QDs often results in a decrease in quality as their synthesis methods are less well developed. In this study, a dropcast film of QDs was used to measure the surface temperature of resistors with different resistivity in a series of circuits by taking a fluorescence image. The difference in resistivities caused differences in surface temperatures at each resistor, resulting in different emission intensities of the QDs coating their surfaces (figure 6). Both millimeter- and micrometer-sized circuits were measured, showing the potential for using QDs as temperature sensors with micrometer resolution and low error (1.9%). This is of interest especially for monitoring the performance of micro- and nano-electromechanical systems (MEMS/NEMS) and integrated circuits (ICs), where temperature often impacts performance. It is also a way to detect defects smaller than the resolution of thermocouples and thermal infrared imagers.

4.2. Ion sensing with QD quenching

Multiple groups have observed that QD PL can change significantly in the presence of ions, often rather specifically, making QDs themselves viable ion sensors [13, 16, 98–101]. In the typical case, such as the ion sensor described by Chen *et al*, QD emission is quenched in the presence of Cu^{2+}, but unresponsive to other cations like Na^{+}, Ca^{2+} and Mg^{2+} [13]. While the majority of the reports demonstrate the dose-dependent photophysical changes in the presence of free ions, few have followed up with experiments to elucidate the exact mechanism of these changes. In cases where ions adsorb to the surface of the QDs, QD emission can be enhanced by ions passivating surface defects [14]; alternatively, QD emission can decrease from ions creating surface states that are effective pathways for non-radiative recombination, quenching the QD [15, 102]. Change in PL intensity, however, also changes with QD concentration, so sensors with a single wavelength readout can be prone to error if calibration is not done before every measurement.

By using two QD emitters, this ion sensing mechanism can be incorporated into a more robust ratiometric ion sensing construct that is less prone to error due to changes in particle concentration. In one such design, large silica nanoparticles were used as a scaffold with red-emitting CdTe/CdS QDs protected within the interior and green-emitting CdTe/CdS QDs attached to the surface, thus exposed to the surrounding environment [15]. In the presence of Hg^{2+} ions, the green QDs on the surface were quenched, resulting in a change in the ratio of red and green emission intensities. By measuring the PL lifetime of the green surface QDs, the authors found that the lifetime decreased from 25.5 to 6.5 ns while the lifetime of the red QDs remained unchanged. The decrease in

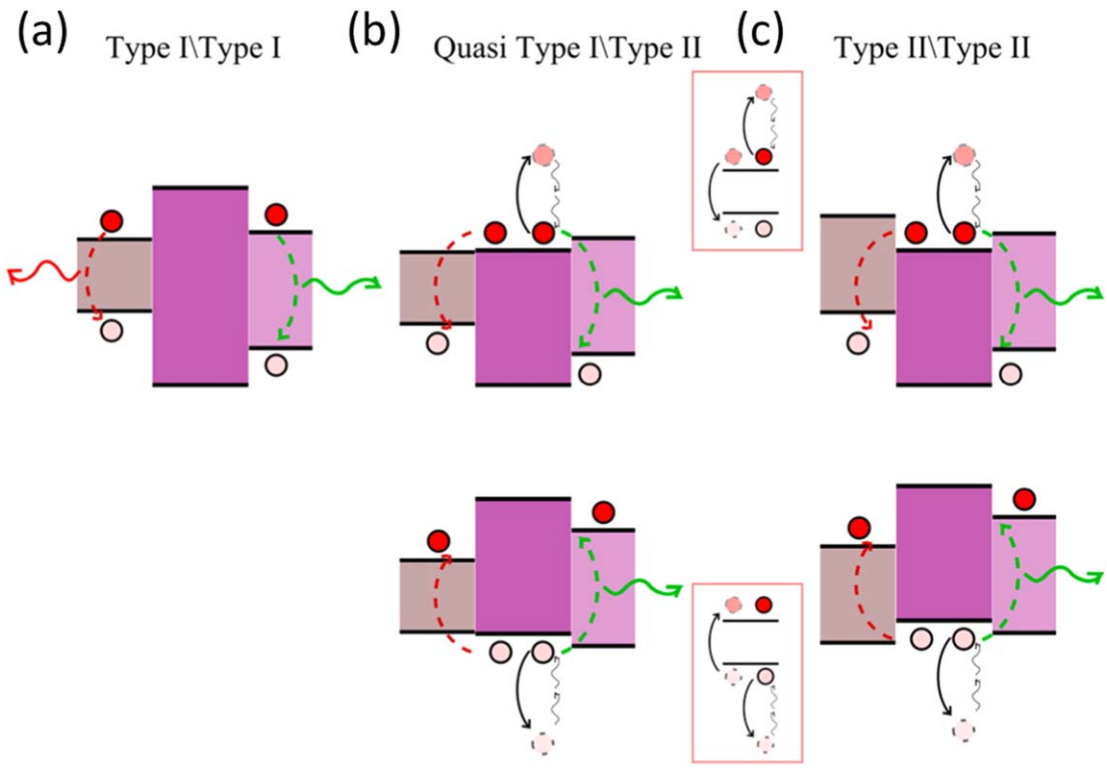

Figure 9. Bandgap alignments that result in dual emission for double quantum dots. (**a**) Type I/Type I emitters contain two electron hole pairs spatially and energetically separated by a wide bandgap barrier resulting in simultaneous dual emission. (**b**) Quasi Type I/Type II and (**c**) Type II/Type II alignments result in a double well for either the electron or hole. One of the charge carrier pairs is non-radiatively lost through Auger processes and the emission color switches stochastically as a result. Reproduced from [114], published under an ACS AuthorChoice License. DOI: 10.1021/acs.accounts.5b00554.

lifetime of the surface QDs indicated that the Hg^{2+} ions were adsorbed onto the surface of the green QDs, initiating charge transfer [102]. Further verification was done by taking absorption spectra of the QDs, showing a 10 nm red-shift of their first excitonic absorption peak. While quenching of the green QDs was seen in the presence of other divalent cations, none showed as significant a change in color as with Hg^{2+}. However, a similar sensor design using CdTe QDs was found to also exhibit green emission quenching in the presence of gold nanoparticles [103], indicating a weakness in the sensor specificity. Wang *et al* attempted to improve specificity by chemically etching the surface CdSe QDs with EDTA (figure 7) [16]. Cadmium on the surface of the QD is chelated by EDTA and Cd^{2+} cavities are left on the surface. QDs exposed to EDTA exhibited a 5 nm blue shift in emission wavelength along with decreased emission intensity. In the presence of Cd^{2+} ions, the cavities on the surface of the QD are filled, resulting in a re-brightening of the QDs as well as a red-shift in wavelength. This chemical etching strategy had been previously applied for ion sensing [14, 17], but the two-color silica nanoprobe design allowed for a ratio-metric output. This sensor was, however, still not completely selective, as the presence of Zn^{2+} ions also increased the PL intensity of the exposed QDs. The authors did not note if the PL wavelength shift was different in the presence of Zn^{2+} or Cd^{2+} ions, a metric that might convey more information about the ions present.

4.3. Intrinsic QD photophysics for voltage sensing

QDs exhibit changes in their photoluminescent properties in response to an electric field due to the quantum-confined Stark effect (QCSE). In QCSE, the presence of an electric field shifts the electron and hole wavefunctions along the field gradient, reducing the overlap integral between them [104]. This leads to an increased PL lifetime, red-shifting of the emission peak, and a decrease in the overall emission intensity [105].

The QCSE was demonstrated in quantum wells [104, 106, 107] before Ekimov *et al* demonstrated the effect in quantum dots. Using glass-embedded CdS and CdSe QDs, the authors showed a 10 meV redshift in the absorption edges of the QDs while applying electric fields up to 100 kV cm^{-1} [108]. To verify QCSE in quantum dots, Empedocles and Bawendi used single QD spectroscopy, eliminating the inhomogeneous broadening of emission spectra that often characterizes ensemble measurements [109]. To accomplish this, they deposited CdSe or CdSe/ZnS QDs of various sizes (4.4 nm to 7.5 nm) onto patterned electrodes and acquired single particle spectra with a far-field epifluorescence microscope cooled to 10 K. With this setup, the authors showed emission shifts as large as 75 meV after applying electric fields of

350 kV cm^{-1}. Other groups extended these low temperature single-QD spectroscopy results, showing red-shifting as well as the expected decrease in photoluminescence intensity with increasing electric fields for type I QDs [110] and type-II quantum rods [111].

Harnessing the QCSE for sensing electric fields in practical applications (such as an action potential in neurology) requires that a sizable change in PL peak position or intensity occurs *at room temperature or higher*. Noting that different geometries, compositions, and band alignment structures can all effect QCSE, Park *et al* screened the single-QD change in emission for eight nanoparticle types in the presence of an electric field [112]. These nanoparticles included two homogeneous type I quantum rods of varying lengths, two quasi-type II quantum rods of different lengths, two type II QDs, and two asymmetric heterostructures. This systematic study allowed the authors to tease apart several variables, uncovering several interesting results. First, for homogeneous type I quantum rods, increasing the length did not change the average shift in the electric field, indicating that there was incomplete charge separation along the rod. Second, rod-shaped geometry showed greater shifts in an electric field than symmetric core/shell geometry, consistent with previous reports [111]. Finally, they demonstrated that type II asymmetric rods exhibited the most significant response, with some individual particles exhibiting a roughly linear response to the electric field culminating in a 13 nm red-shift in the emission peak and 36% drop in PL intensity in response to a 400 kV cm^{-1} field.

These results encouraged others to assess the ability of QDs to respond to physiologically relevant electric field strengths (~100 kV cm^{-1}). Marshall and Schnitzer used numerical finite basis methods to model spherical QDs and the tunneling resonance method to model heterostructured quantum rods, and calculated the response of each to the electric field changes induced by a typical action potential [113]. They found that type II and quasi-type II heterostructures exhibit greater voltage sensitivity than spherical geometries, consistent with the results above from Park *et al.* They calculated that CdTe/ZnTe quantum rods would produce a five-fold greater percent change in PL lifetime ($\Delta\tau_r/\tau_r$) than CdTe/ZnS core–shell structures. However, this enhancement is highly sensitive to the minimal valence band offset between the two materials; similar heterostructures with a larger offset (such as CdTe/CdSe) showed less responsiveness to voltage due to having less polarizable holes. It is also worth noting that these simulations are contingent upon perfect orientation of the quantum rods perpendicular to the electric field.

Using signal detection theory, Marshall and Schnitzer also assessed the feasibility of using the QCSE in QDs to detect single spikes in neurons compared to voltage-sensitive dyes (VSDs) and genetically encoded voltage indicators (GEVIs). They showed that even type I spherical CdTe QDs in the cell membrane would outperform contemporary VSDs and GEVIs in detecting action potential spikes, even at concentrations orders of magnitude lower than VSDs and GEVIs. These modeling results, however, were based on comparisons to a GEVI (*i.e.*, ArcLight) and VSD (*i.e.*, hVOS) that are now outdated compared to the current best-in-class GEVIs and VSDs.

A recent report by the Weiss group was the first to harness QCSE in quantum rod heterostructures *in vitro* in HEK293 cells [18]. They designed quasi-type II CdSe-seeded CdS rods with hydrophobic and hydrophilic peptide coatings to align the rods perpendicular to the electric field (figure 8). This novel attempt to orient rods in the membrane and measure voltage yielded interesting, but somewhat disappointing, results. The quantum rods were able to respond to the electric discharge of HEK cells, but were nearly an order of magnitude less sensitive than ANEPPS (a common VSD), and exhibited significantly noisier signals. The authors point to the challenge of inserting the rods perpendicular in the field: only 16% of their rods were oriented properly, indicating the challenge of controlling rod insertion into the cell membrane.

4.4. Dual-color intrinsic quantum dot sensors

Changes of PL intensity alone can be a poor sensor output as other events, such as a change in QD concentration, particle aggregation, or other changes in the environment, may also result in a change in emission intensity. Ratiometric measurements that monitor the change of the ratio of PL intensity at two different wavelengths are generally preferred to single color measurements because they are less sensitive to environmental factors. Dual color sensors can exhibit uncoupled or coupled emission, whereby the second color acts either as a constant emitter for normalization of the variable emission or exhibits variable emission with inversely proportional changes in emission intensity to the first emitter, respectively. In the former case, the consistent emission intensity of the secondary color is used as a control in the system, whereas in the latter case, the secondary color intensity enhances the effective change in signal in response to the stimulus. In this section, dual emitting quantum dots and their use as sensors is briefly discussed. Other dual-color sensors operating on the principle of energy transfer will be covered in sections 5 and 6.

4.4.1. Dual emitting quantum dots

The creation of a single nanoparticle that exhibits two emission colors is interesting from both a fundamental and applications perspective. Synthesis of QD-dual emitters is achieved by: (1) growing core/shell/shell QDs with materials that result in a quantum dot-

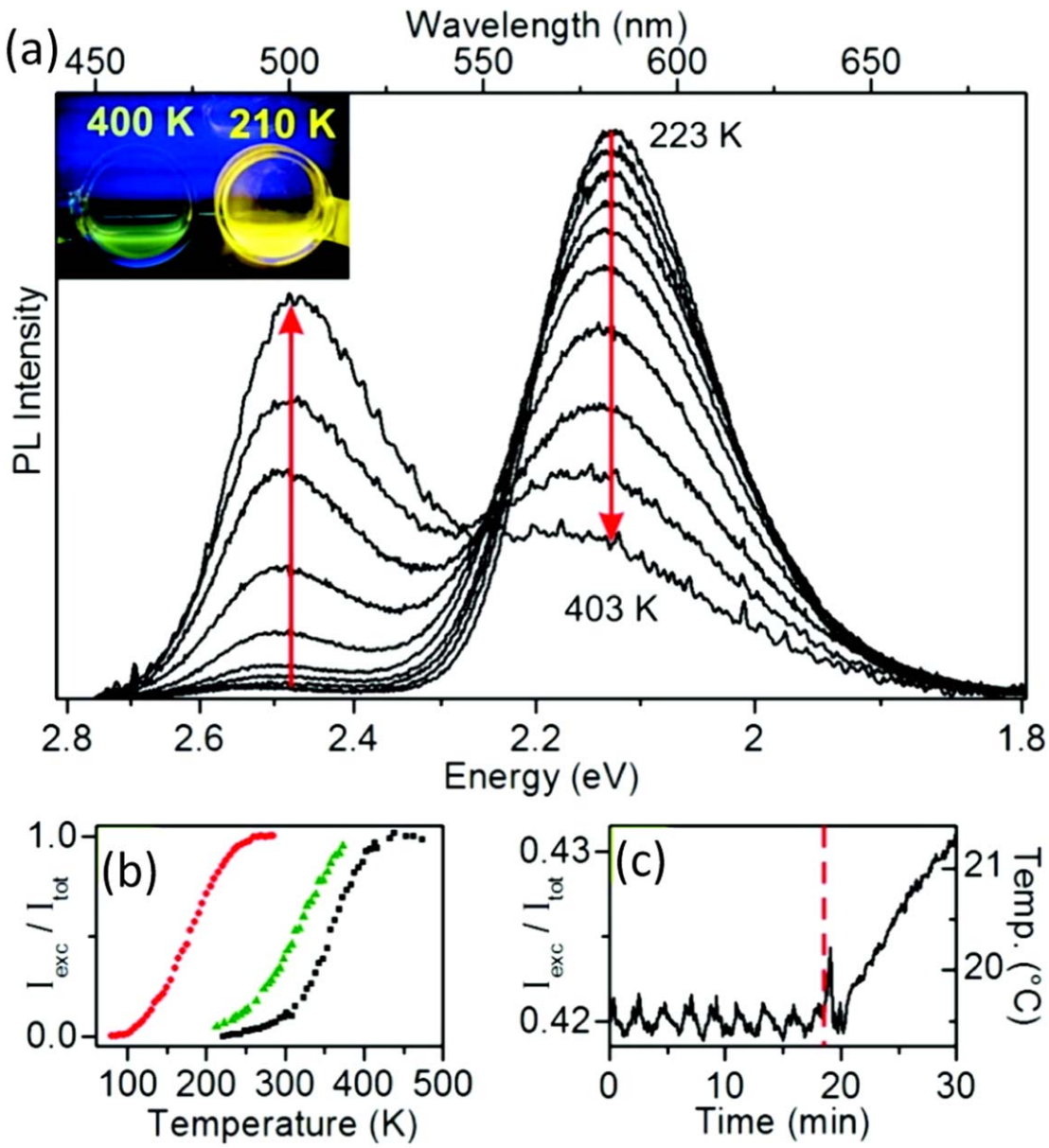

Figure 10. Fluorescence change as a function of temperature for $Zn_{1-x}Mn_xSe/ZnCdSe$ QDs. (**a**) The ratio of exciton emission and dopant emission changes as a function of temperature. Inset: picture showing visible color differences at two temperatures. (**b**) Temperature response curves for three QDs with different core/shell dimensions demonstrate the tunability of the QD heterostructure design for temperature sensing in different temperature regimes. (**c**) PL of a QD sensor cooled to 19 °C. The red dotted line indicates the removal of the coolant. The sensor subsequently warmed, resulting in an increase in the ratio. Reprinted with permission from [124]. Copyright 2010 American Chemical Society.

quantum well (QD-QW) band alignment, (2) growing seeded quantum rods (QRs) tipped with a second material, or (3) including dopants during nucleation or growth. Quantum dots that fall in the first two categories are dubbed double quantum dots and exhibit unique optoelectronic properties including intraparticle charge transfer and luminescence upconversion [114]. Core/shell/shell heterostructures that result in dual emission are shown in figure 9.

Type I/Type I emitters consist of an energy barrier sandwiched between the core and outer shell. For example, several CdSe/ZnS/CdSe dual emitters have been reported [115–118]. In Quasi-Type I/Type II dual emitters like the CdSe/CdS/ZnSe heterostructure [119], the nominal energy offsets in either the conduction or valance band create a double well for either the excited electron or hole charge carrier, respectively. Since the probability of emission of more than one photon is low due to the likelihood of non-radiative Auger recombination, the emitted photons stochastically switch between the two possible emission colors. Type II/Type II emitters work similarly and include PbS/zbCdSe/wzCdSe/CdS [120] heterostructures, where the difference in crystal structure of the same material results in a bandgap offset at the core/shell interface. Similarly, Zhao *et al* [121] synthesized PbS cores with a cation-exchanged zinc-blende (zb) CdS shell before depositing a thick wurtzite (wz) CdS layer on top. The zb CdS shell served as a potential barrier between the PbS core and wz CdS shell,

resulting in red emission from the core and bue emission from the shell.

So far, double dots have generated interest as optical gain media [115] and upconversion platforms [120], but the dual emission can also be used for sensing. For example, the PbS/ CdS QDs described above were embedded in poly(methyl methacrylate) (PMMA) films to measure PL temperature dependence [122]. Emission from both the core and shell increased as temperature decreased. Unsurprisingly, the temperature dependence was not the same between the different materials, resulting in a change in the ratio of blue and red emission.

Another example of a dual color intrinsic sensor was demonstrated by Razgoniaeva *et al* [123]. A double well PbS/CdS/CdSe heterostructure was synthesized that exhibited emission from the PbS core as well as from the CdSe outer shell. The authors then investigated how the presence of methyl viologen (MV^{2+}) and 3-mercaptopropionic acid (MPA) changed the PL emission profile of the QDs. MV^{2+} quenched PbS emission much more efficiently than CdSe emission as a result of the long PbS PL lifetime when compared to CdSe. The longer PbS fluorescence lifetime results in slower non-radiative processes that allow for quenching at a higher rate. In the presence of MPA, CdSe emission was more efficiency quenched, indicating that the rate of hole transfer from CdSe to MPA is much higher than that of PbS to MPA. For both analytes, one color is quenched more efficiently than the other, so the ratio of emission colors can be used to quantify analyte concentration.

While both of the dual-emitting QD sensors described here have limited long-term application potential because they contain multiple toxic constituents (Pb and Cd), the idea of using a barrier between the core and shell of a QD to create dual emission for use as a temperature sensor could also be explored with more environmentally friendly compositions currently being developed.

4.4.2. Doped QDs for dual-color sensors

Doped QDs provide the opportunity to develop QD-based temperature sensors with ratiometric fluorescent readouts. The presence of dopants in a QD introduces additional energy levels, and, depending on where the dopant levels lie relative to the valance and conduction bands of the QD, some structures exhibit dual emission from a single QD. If the ratio of fluorescence intensity between the two peaks is temperature sensitive, ratiometric calibration of peak intensities with regard to temperature is possible.

An excellent example of this was demonstrated when Vlaskin *et al* developed $Zn_{1-x}Mn_xSe$/ZnCdSe QDs with dual emission [124]. Dopant loading in the core was controlled and the QD bandgap was tuned relative to the dopant levels by changing shell thickness. Their QDs showed a large change in the ratio of exciton versus dopant emission when temperature was varied (figure 10(a)); in addition, the temperature range for sensing could be tuned by changing the dimensions of the core and shell. To demonstrate this, three QDs with differing core/shell dimensions were synthesized that showed temperature dependent color change across a temperature range of 100–400 K (figure 10(b)). The measurements were repeatable through three temperature cycles. To further highlight the advantage of ratiometric sensing, they transferred their QDs from toluene to heptane, decreasing overall QY by ~50%. While the intensity of the QDs decreased as a result, the ratio of the two emission colors was identical.

Other dual emission QDs used in nanothermometry include Mn-doped CdSSe/ZnS core/shell QDs [19], ZnMnSe/ZnS/CdS/ZnS QDs [125], and alloyed ZnCdMnSe QDs [126]. Ag- and Mn- co-doped [20] or Cu- and Mn- co-doped ZnInS QDs are more recent examples that extend this premise to heavy metal-free compositions [127].

5. QDs in Förster resonance energy transfer

The sensors discussed above exhibit a change in PL intensity due to a change in QD concentration or an environmental force altering the QD photophysics. Arguably the most common sensing mechanisms, however, involve energy transfer mechanisms to another molecule. Several energy transfer mechanisms exist and can be classified generally into two categories: resonance energy transfer (RET) or electron transfer (eT). An exceptionally comprehensive review on energy transfer involving QDs has been recently published [26]. Here we will more succinctly highlight energy transfer mechanisms and applications in sensing.

The most prominent energy transfer mechanism in biosensing is Förster, or fluorescence, resonance energy transfer (FRET), a distance-dependent non-radiative energy transfer from a donor to acceptor chromophore through dipole-dipole resonance. Because FRET uses two chromophores, ratiometric sensing is often built in, with the exception of systems where the acceptor is non-fluorescent (*i.e.*, a quencher). As previously discussed, ratiometric sensing is often advantageous to single color sensing for internal calibration and enhanced sensitivity. In FRET sensors, one can monitor both the efficiency of energy transfer from the donor to the acceptor as well as the resulting changes in the acceptor-donor emission ratio. Factors affecting FRET efficiency include (1) the donor-acceptor separation distance, (2) the spectral overlap between the acceptor and donor, (3) the quantum yield of the donor, and (4) the alignment of the donor and acceptor dipoles. The ratiometric measurement is furthermore impacted by the quantum yield of the acceptor molecule and analysis can be complicated by overlap between the donor and

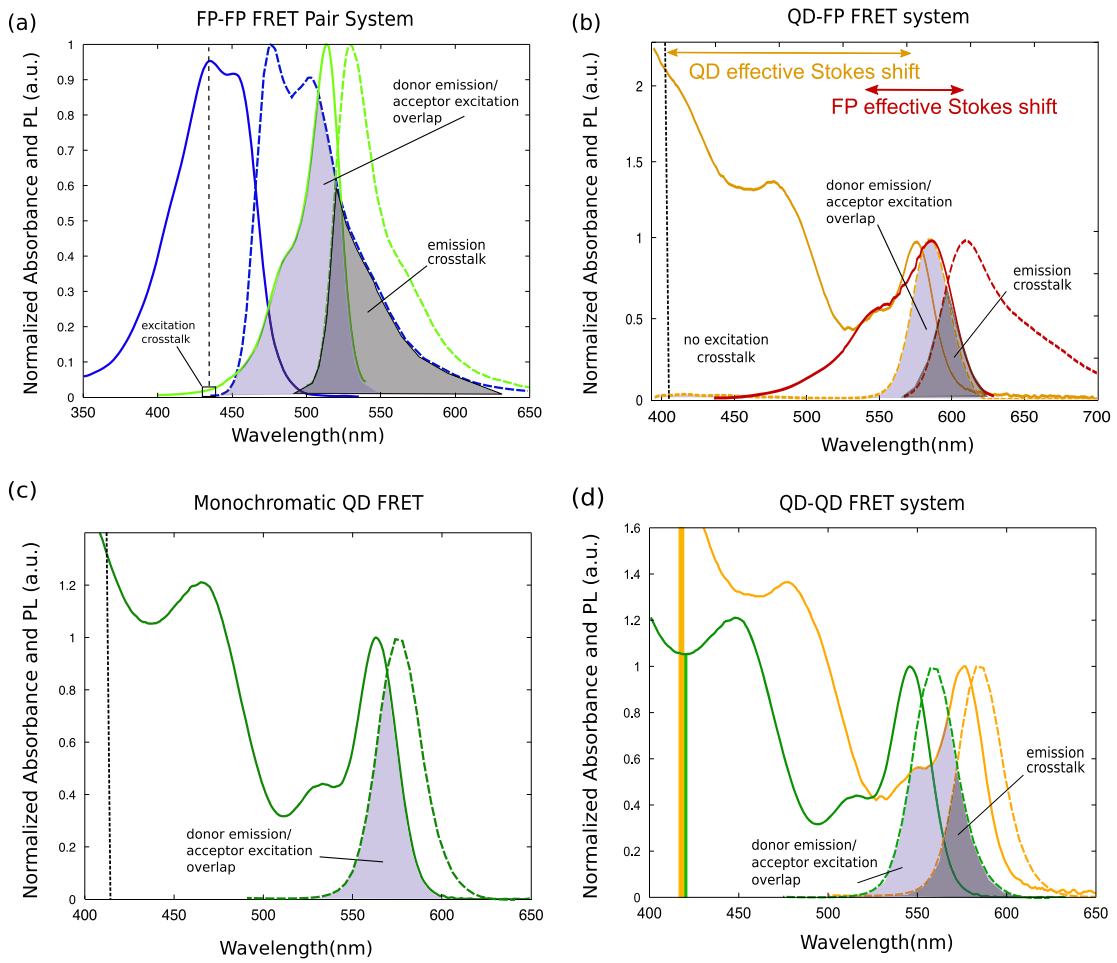

Figure 11. The absorption and emission spectra for (**a**) a pair of fluorescent proteins (FP-FP) and (**b**) a QD-FP FRET pair. Excitation crosstalk is avoided in the FP-FP case by choosing FPs with suboptimal spectral overlap, whereas the large Stokes shift of the QD allows for zero excitation crosstalk in a QD-FP pair and perfect overlap of the donor emission and acceptor excitation. In panel (**b**) the FP effective Stokes shift when exciting away from its excitation maximum is indicated. While exciting away from the FP excitation maximum can decrease crosstalk, sensor brightness will suffer. Panels **a** and **b** are also representative of FRET pairs using fluorescent dyes. (**c**) Spectral overlap in the QD absorption and emission spectra can lead to homo-FRET. (**d**) Two color QD-QD FRET results in significant direct excitation of the acceptor. Adapted from [41]. Distributed under a Creative Commons Attribution Non-Commerical License 4.0 (CC BY-NC).

acceptor emission peaks. For energy transfer to occur, acceptor absorption must overlap with the donor emission wavelengths. The degree of this overlap is defined as the spectral overlap integral, J^{λ} [31, 128]:

$$J^{\lambda} = \int f_D(\lambda)\, \varepsilon_A(\lambda)\, \lambda^4 d\lambda \tag{3a}$$

$$f_D = \frac{F_D(\lambda)}{\int F_D(\lambda)\, d\lambda} \tag{3b}$$

where $f_D(\lambda)$ is the fluorescence spectrum of the donor normalized to 1 by dividing by its total area (equation (3b)), and $\varepsilon_A(\lambda)$ is the molar absorptivity of the acceptor, all scaled to wavelength, λ; J^{λ} has units of M^{-1} cm^{-1} nm^4. To compare the expected performance of potential donor-acceptor pairs, one uses the overlap integral to calculate the Förster distance, R_0, *i.e.*, the donor-acceptor distance at which 50% FRET efficiency is observed [31]:

$$R_0 = \left[\frac{9 \ln 10\, \kappa^2 \Phi_D\, J}{128\, \pi^5\, n^4\, N_A}\right]^{\frac{1}{6}} \tag{4a}$$

$$R_0(\mathrm{nm}) = 0.02108\left[\frac{\kappa^2 \Phi_D}{n^4}\left(\frac{J^{\lambda}}{\mathrm{M^{-1}cm^{-1}nm^4}}\right)\right]^{1/6} \tag{4b}$$

where κ^2 is the dipole orientation factor between the donor and acceptor, Φ_D is the quantum yield of the donor, and n is the solvent refractive index (all unitless terms). The dipole orientation factor κ^2 can span from 0 to 4, with a value of 0 for no dipole overlap and 4 for perfectly aligned dipoles. In FRET sensors where the chromophore dipoles are randomly oriented over time, $\kappa^2 = 2/3$ is used. The units used to calculate R_0 can differ, so the expression that uses spectral overlap integrated over wavelength is also shown (equation 6) in order to avoid confusion in choice of units. If R_0 is

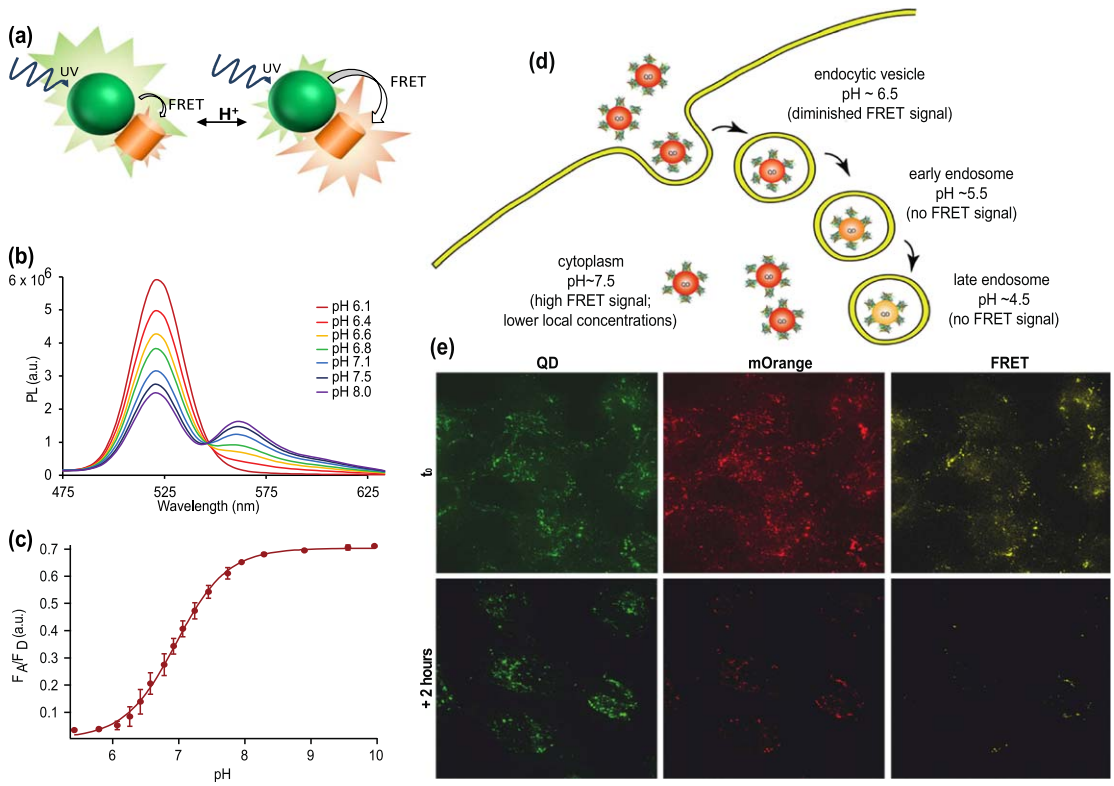

Figure 12. QD-FRET-based pH sensor for intracellular imaging. (**a**) Schematic of ratiometric pH sensor based on change in absorption cross-section of acceptor fluorescent protein mOrange in response to pH. At alkaline pH, mOrange is optically active and acts as an efficient FRET acceptor, siphoning energy from the QD donor. At acidic pH, the mOrange is not optically active, and FRET is diminished, resulting in higher emission intensity from the QD. (**b**) Change in PL emission upon titration of the FRET sensor. The donor QD emission is highest with little FRET evident at pH 6.1. At more alkaline pHs, energy transfer results in a decrease in QD donor emission intensity and increase in mOrange acceptor emission intensity. (**c**) Plot of the acceptor emission intensity to donor emission intensity versus pH creates a calibration curve for the ratiometric sensor. (**d**) Schematic of how changes in energy transfer efficiency results in changes in emission color as the fluorescent probe progresses through the endocytotic pathway. (**e**) After brief exposure to cells (t_0) FRET is evident in epifluorescence microscopy. After 2 h, endocytosed probes are exposed to a more acidic environment and exhibit substantially reduced FRET. Adapted with permission from [132]. Copyright 2012 American Chemical Society.

known, the FRET efficiency of a system at a specific donor-acceptor separation, r_{DA}, can be calculated [31]:

$$E_{FRET} = \frac{1}{1 + \left(\frac{r_{DA}}{R_0}\right)^6} \tag{5}$$

Experimentally, FRET efficiency can be monitored through change in donor fluorescence intensity or fluorescence lifetime [31]:

$$E_{FRET} = 1 - \frac{F_{DA}}{F_D} = 1 - \frac{\tau_{DA}}{\tau_A} \tag{6}$$

where F_{DA} (τ_{DA}) is the fluorescence intensity (lifetime) of the donor in the presence of an acceptor, and F_D (τ_D) is the fluorescence intensity (lifetime) of the donor in the absence of energy transfer. By experimentally monitoring the fluorescence of a FRET system, one can use the changes in PL intensity or lifetime to determine the FRET efficiency, and thus donor-acceptor distance, or use knowledge of the sensor configuration (donor-acceptor distance) to predict the sensor FRET efficiency.

While FRET can occur between any two chromophores, there are a few advantages of using QDs as FRET donors. In addition to the overarching theme of QD PL being brighter and more photostable than dyes, the unique spectral profile of QD FRET donors can be used to reduce crosstalk. Due to the shorter effective Stokes shift of most organic emitters (including fluorescent proteins), challenges arise with maximizing spectral overlap for high FRET efficiency while minimizing excitation and emission crosstalk. If an excitation wavelength is chosen to minimize excitation crosstalk such that only the donor dye or protein is excited, the overall brightness of the system is decreased, as it requires that the donor is excited away from its absorption maximum. In contrast, QDs have broad absorption in the UV with increasing molar extinction coefficients at higher energies, *i.e.*, in the UV and blue wavelength range. In this context, photoexcitation far from the QD emission peak (and the acceptor absorbance) leads to enhanced absorption by the QD, creating a brighter system. Figure 11 illustrates the differences in spectral overlap between various donor-acceptor systems [41].

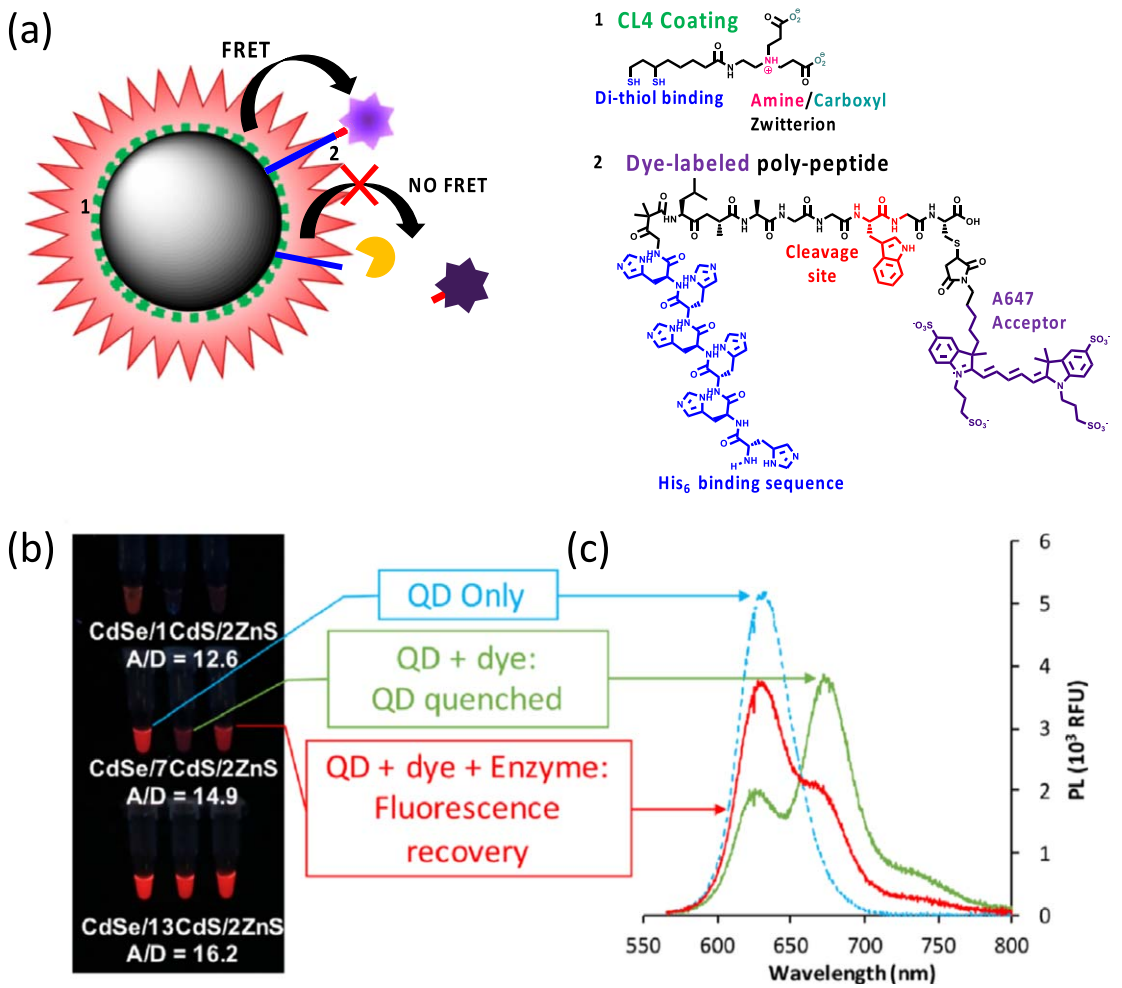

Figure 13. In a typical enzyme cleavage assay, his-tagged, dye-labeled peptides are self-assembled to the QD donor, quenching QD emission via FRET. In the presence of enzyme, the peptide is cleaved, terminating FRET efficiency and resulting in re-brightening of the QD emission. Panel (**a**) shows a schematic of FRET-based enzyme sensing and panel (**b**) shows images of sensors using QDs of different sizes as donors. Only the medium-sized donor shows visible changes in brightness after addition of enzyme, while all sensors can be monitored by taking PL using a fluorimeter (**c**). Adapted from [25] with permission from The Royal Society of Chemistry.

5.1. FRET sensors using QD donors

As with the fluorescently labeled QD sensors described in the first section, FRET sensors using QDs benefit from the large surface area that provides a base for a multitude of functionalization schemes. This is well demonstrated in an early report from Suzuki *et al* [129]. They functionalize the surface of commercially available QDs with ssDNA, dsDNA, fluorescein-5, and GFP to make DNase, DNA polymerization, pH and proteolytic FRET sensors respectively. The authors also highlight that using QDs as FRET donors provides a pathway for single excitation wavelength multiplexing and show that by mixing their nuclease and protease sensors they can monitor both sensing events simultaneously as long as QDs of different and distinguishable emission wavelengths are used for each. While the discussion of these sensors is largely qualitative, the possible breadth of applications for QD-FRET-based sensing was effectively demonstrated.

One way to use FRET for sensing is to utilize changes in the optical properties of the acceptor molecule to generate a responsive change in FRET efficiency through changes in the spectral overlap. There are a couple of examples of this mechanism in pH sensing based on the organic fluorophores squarine [130], SNARF [131], or variants of the fluorescent protein mOrange [132]. In the case of the QD-mOrange pair, the absorption cross-section of the FP varied significantly with pH, changing the FRET efficiency, resulting in a 20-fold difference in the ratio of the acceptor emission intensity to the donor emission intensity over a physiologically relevant pH range (pH 6–8) (figure 12). Similarly, the absorption of 2D materials such as molybdenum disulfide (MoS_2) changes in the presence of an electric field, facilitating their use as FRET acceptors in devices that can sense changes in applied field [133].

The most frequently used FRET designs sense a change in distance between the donor and acceptor pair, r_{DA}. FRET efficiency is highly distance dependent (equation (5)), and therefore changes in r_{DA} on the nanometer scale can be monitored. Because FRET

efficiency is negatively impacted by increased sensor size, the sizes of the fluorophores used are parameters of interest when designing a FRET probe. Towards that end, the Dennis group performed a systematic study comparing CdSe/xCdS/2ZnS QD donors of varying shell thicknesses with dye-labeled, tryptophan cleavable, his-tagged peptides self-assembled to their surface [25]. By using the same acceptor for every QD, the effect of shell thickness and size on FRET efficiency, and the implications on sensor design were explored. As expected, by using QDs with thicker shells and increased overall size, the maximum FRET efficiency of the probe decreased. However, it was shown that the larger QD size significantly increased brightness, with the brightest samples being almost 8-fold brighter than commercially available QDs emitting at similar wavelengths. As previously discussed, increased fluorophore brightness can be useful for POC applications where cost and ease of detection are a concern. While all sensors were able to detect the presence of tryptophan when using a fluorimeter for measuring fluorescence, only the sensor using a medium sized QD (diameter ~9 nm) was able to show visible changes in fluorescence after the addition of tryptophan, as it was both bright enough for facile visual detection and still small enough for efficient energy transfer (figure 13) [25].

The r_{DA} of a pre-assembled construct can change when the sensor undegoes a conformational change, complete dissociation, or displacement of the acceptor from the donor. The sensor described above uses an enzyme cleavable peptide to mediate acceptor displacement as a measure of enzymatic activity. QD-FRET has been widely demonstrated for enzyme sensing [23, 25, 28, 34, 134–138]. Proteolytic activity can be monitored by attaching acceptors to quantum dot donors with an enzyme cleavable peptide. Frequently, dye-labeled peptides containing a histidine region and enzyme cleavable sequence are self-assembled to QDs as FRET acceptors, quenching the PL of the QDs [23, 25, 28, 34, 135, 136]. In the presence of enzyme, the peptide is cleaved releasing the acceptor from the QD and reducing FRET, as observed through the enhancement in QD PL intensity [135]. Changes in the PL over time can be used to calculate kinetic parameters of substrate digestion through Michaelis-Menten (MM) kinetic formalism. Similarly, fluorescent proteins (FPs) can be engineered to include enzyme cleavable linkers to achieve the same effect [134]. In 2012, Algar *et al* performed a more detailed study tracking the number of peptides per QD over time and showed that substrate digestion deviates from predicted MM formalism. A hopping mode of activity was described, whereby the enzyme consumes multiple substrates on a QD surface before relocating to a new QD, causing an initial enhancement in the rate of digestion [136]. Diaz *et al* [137] explored this further by creating QD-dye proteolytic FRET sensors for both elastase and collagenase. They found that elastase was well represented by the MM model whereas collagenase was not, demonstrating that while QD-dye FRET protease sensors can be used for enzyme detection, the kinetics of these reactions can be variable.

Acceptor displacement can occur through processes other than enzyme cleavage—for example, QD FRET-based immunoassays [139, 140]. These have similar design aspects to QD FLISAs, but the QD is used as both a platform and FRET donor. In this scheme, the sensor does not need to be attached to a substrate but is instead measured directly in solution. This is advantageous in that is does not require long incubation times or multiple washing steps. For example, Kattke *et al* optimized a QD-FRET system for the detection of Aspergillus mold spores even in a solution with high background autofluorescence [140]. A QD donor was conjugated to IgG antibodies and incubated with quencher-labeled analytes, resulting in a FRET-based decrease of QD PL. The presence of the target analyte displaced the quencher-labeled analyte, resulting in QD fluorescence recovery.

5.2. FRET sensors using QD acceptors

As already exemplified in this review, QDs are generally used as FRET donors due to their bright emission and broad absorption. According to the Förster formalism, non-radiative energy is transferred from an excited donor molecule to an acceptor molecule in its ground state when they are in close enough proximity. The broad excitation profile and relatively long PL decay times for QDs compared to traditional fluorescent dyes ($\tau_{QDs} \sim$ 5–100 ns versus $\tau_{dyes} \sim$ 1–5 ns) hinders the use of QDs as FRET acceptors. Upon photoexcitation, both the dyes and QDs are excited, with the QD remaining in an excited state than much longer the dye, precluding energy transfer [141–143]. The introduction of luminescent lanthanides as FRET donors with up to millisecond lifetimes change this dynamic by utilizing a FRET donor with a PL lifetime much longer than that of the QD acceptor [35, 36]. By collecting PL lifetimes in time gates much longer than the natural decay of the QD, but still within the lifetime of the lanthanide decay, the direct excitation of the QD and any background autofluorescence are not recorded, greatly simplifying analysis of the system.

Lanthanide emitters can be incorporated into FRET devices in the form of molecular complexes or lanthanide-doped upconverting nanoparticles. Time-resolved spectroscopy is used to record the luminescence intensities of FRET pairs in individual detection channels in time-gated mode after pulsed excitation. If the lifetime of the acceptor is much shorter than the lifetime of the donor, the lifetime of the donor in the presence of acceptor can be assumed to be the same as the lifetime of the acceptor in the presence of the donor ($\tau_{DA} = \tau_{AD}$ for $\tau_A \ll \tau_D$). Time-gated detection of fluorophores with long luminescence lifetimes

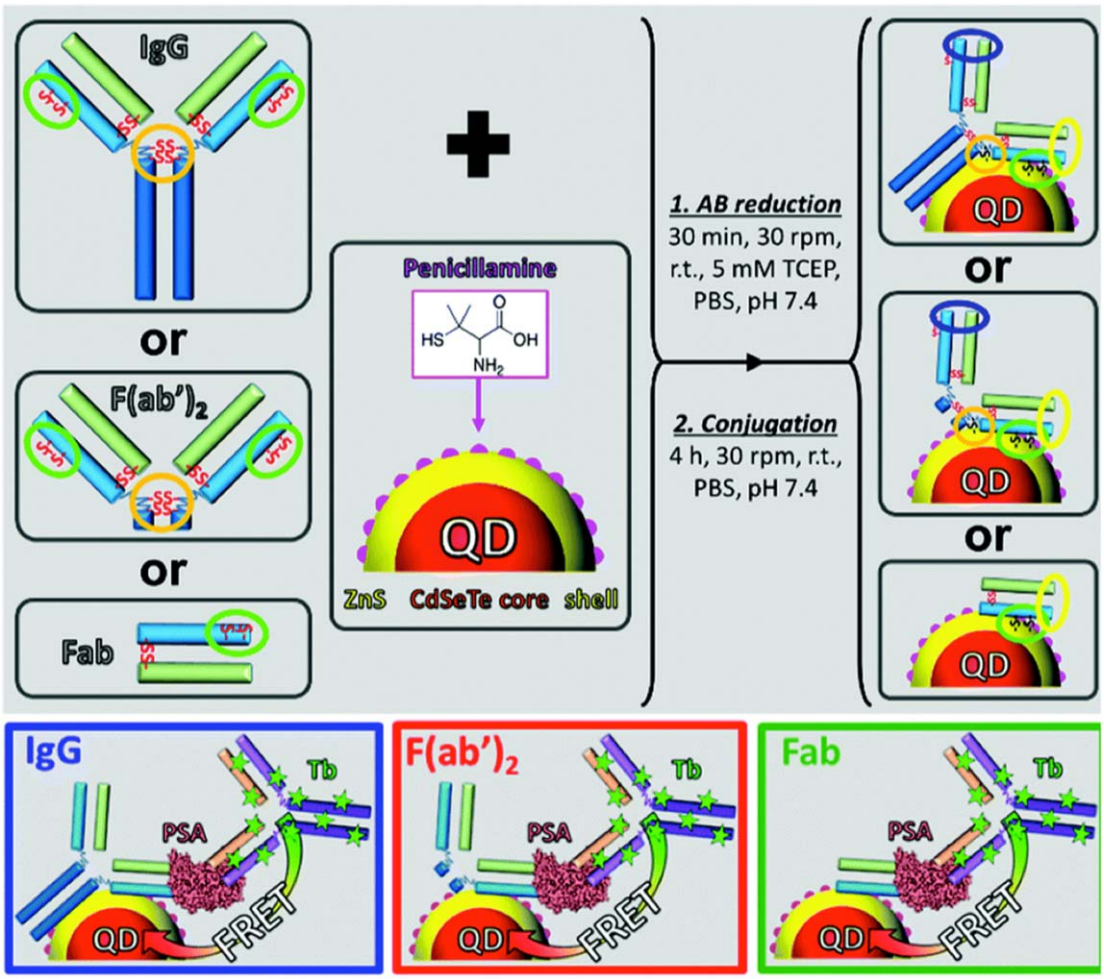

Figure 14. (**top**) Direct conjugation of thiol-antibody (fragments) to the surface of compact QDs via metal affinity of thiol to Zn. (**bottom**) When the antigen PSA is introduced in the system, both the QD-antibody (fragment) and L4Tb-IgG bind PSA, bringing the L4Tb and QD into close proximity, resulting in FRET. Adapted from [155] with permission from The Royal Society of Chemistry.

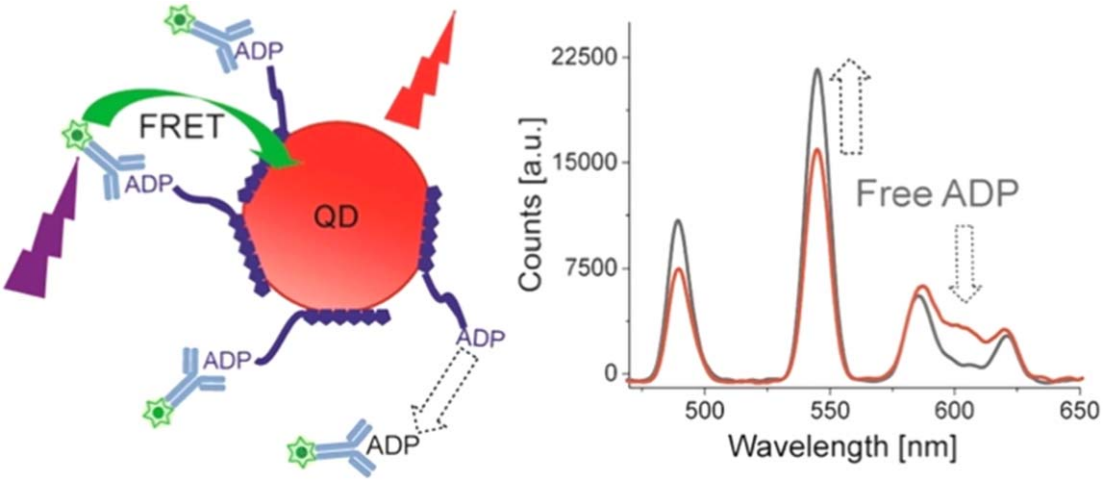

Figure 15. (**left**) Schematic representation of His6-ADP self-assembly on Zn^{2+} surface of QD and Tb labelled antibodies recognizing ADP. (**right**) Upon UV excitation, FRET from Tb to the QD results in quenching of the Tb emission and sensitization of the QD emission (red curve). Upon addition of free ADP, the Tb-antibody detaches from the QD causing a decrease in QD emission and increase in Tb emission (black curve). Reprinted with permission from [21]. Copyright 2018 American Chemical Society.

efficiently suppresses interference from biological autofluorescence as well as directly excited FRET acceptors [29, 143]. Therefore, a ratiometric output for biological assays can be used to quantify the biomolecule of interest, while also suppressing sample and excitation source fluctuations [35, 144]. The

sensor output is the ratio of the time-gated photoluminescence intensities of the FRET acceptor and FRET donor in the presence of the donor and acceptor, respectively, over a defined time period:

$$sensor\ output = \frac{\int_{t1}^{t2} I_{AD}\ dt}{\int_{t1}^{t2} I_{DA}\ dt} \quad (7)$$

where $\int_{t2}^{t1} I_{AD}\ dt$ is the time gated PL intensity of the acceptor detection channel integrated over a time-window from t_1 to t_2 (μs or ms) measured at its emission wavelength, and $\int_{t2}^{t1} I_{DA}\ dt$ is the time-gated PL intensity of the donor detection channel over a time-window from t_1 to t_2 (μs or ms) measured at its emission wavelength.

In 2005, Hildebrandt *et al* showed that QDs could be used as efficient FRET acceptors when paired with a terbium chelate with a long-lived emission lifetime in the ms range [145]. For this purpose, they designed a time-resolved FRET system based on biotin-streptavidin interaction where CdSe/ZnS QDs with an emission maximum at 655 nm were coated with a biotinylated polymer complex (QD655-biot) and streptavidin was labelled to the terbium chelate through its activated ester group (strep-Tb). Using a fixed concentration of strep-Tb and increasing concentration of QD655-biot, they measured the time-resolved emission of the donor and acceptor following pulsed excitation at 308 nm. The FRET ratio from this system integrated from 0.25–1 ms was dependent on the QD655-biot concentration, strongly suggesting sensitized emission of the QDs in the μs range due to FRET. The analysis of the QD emission decay curve after FRET also revealed the appearance of two new long-lived components arising from strep-Tb. The Tb-to-QD FRET system resulted in improved sensitivity of biotin detection with a picomolar detection limit [145].

Since then, clinically relevant biomarker detection has been demonstrated using time-gated Tb-to-QD FRET in homogeneous bioassays. When using antibodies in FRET based sensors, their large size limits maximum achievable FRET efficiency. Because FRET is highly distance dependent, the FRET efficiencies of QD donor-based immunoassays tend to be low. One route towards alleviating this issue it to use antibody binding fragments instead. Wegner *et al* bioconjugated commercially available QDs from eBioscience (eQDs) and a carbodiimide-functionalized terbium complex (Lumi4-Tb-NHS; L4Tb) from Lumiphore with two distinct monoclonal antibodies (IgG), divalent fragments ($F(ab')_2$), or monovalent antibody fragments (Fab) against prostate specific antigen (PSA) [146]. In the presence of PSA, the QD-antibody (fragment) and L4Tb-antibody (fragment) both bind to the analyte, bringing them in close proximity for FRET. They found that using QD-Fab bioconjugates yielded the highest sensitivity in the QD-Tb FRET system due to the smaller biomolecular size reducing the donor-acceptor distance and a higher labelling ratio. The limit of detection (LOD) of 1.6 ng mL^{-1} PSA in serum samples is significantly lower than the clinical cut-off of PSA of 4 ng mL^{-1} [146]. In a subsequent study, the flexibility of the FRET system was demonstrated using nanobody-eQD650/L4Tb conjugates for the detection of epidermal growth factor receptor (EGFR) in low volume buffer and serum samples with LODs of 23 ng mL^{-1} and 34 ng mL^{-1}, respectively, which are below the recommended clinical cut-off level of 45 ng mL^{-1} [147].

Iterations on the Tb-QD FRET immunoassays helpfully demonstrate the challenges of conjugating complex biomolecules like antibodies to QDs in a way that maintains high binding affinity for the analyte and quantify gains made by using different QD coatings or smaller antibody fragments. Since eBioscience QDs have been discontinued, Bhuckory *et al* developed a standard and simple procedure to conjugate thick PEG-coated QDs from Life Technologies (iQDs) to antibodies and tested their efficacy in a L4Tb-to-QD FRET immunoassay for PSA using Fab and IgG [148]. Disulfide bonds on Fab were reduced to thiols and conjugation to iQD605/655/705 was performed by converting amine-reactive QDs to maleimide-reactive QDs using sulfo-EMCS as a crosslinker. Their results showed a significant increase in the FRET-ratio with increasing concentration of PSA for all three FRET systems. The strongest relative increase in FRET-ratio was observed for the L4Tb-iQD705 FRET pair due to the most efficient FRET with the least L4Tb background, due to its large Förster distance. The three FRET systems exhibited sub-nanomolar LODs of 23 ng mL^{-1}, 3.7 ng mL^{-1} and 2 ng/mL for L4Tb-iQD605, 655, and 705, respectively [148].

In 2016, Mattera *et al* [149] further reduced the size of their biosensor. In their study, they conjugated Fabs to QDs for FRET-based sensing comparing commercially available water-soluble QDs coated with a polymer to the same base QDs coated with a compact, commercially available zwitterion, penicillamine. Two colors of QDs, emitting at 605 and 705 nm, coated with the polymer or with penacillamine were functionalized with Fabs and analyzed for performance in a FRET assay. Sensors utilizing the penicillamine-coated QDs were 6.2-fold and 2.5-fold more sensitive than the 605 nm and 705 nm polymer-coated QDs, respectively. This was attributed to the decrease in overall size of the QD/Fabs when using penicillamine and coincided well with other studies showing that the FRET efficiency between CdSe/ZnS QDs and his-tagged FPs is highly dependent on the ligand used for water solubilization [150, 151]. Other reports of small molecule ligands for water-solubilization have been published [152–154], but none have demonstrated stability over as extended of a time period (2 years) as Mattera *et al* [149]. In a later study, Bhuckory *et al* [155] used the compact QDs as demonstrated by

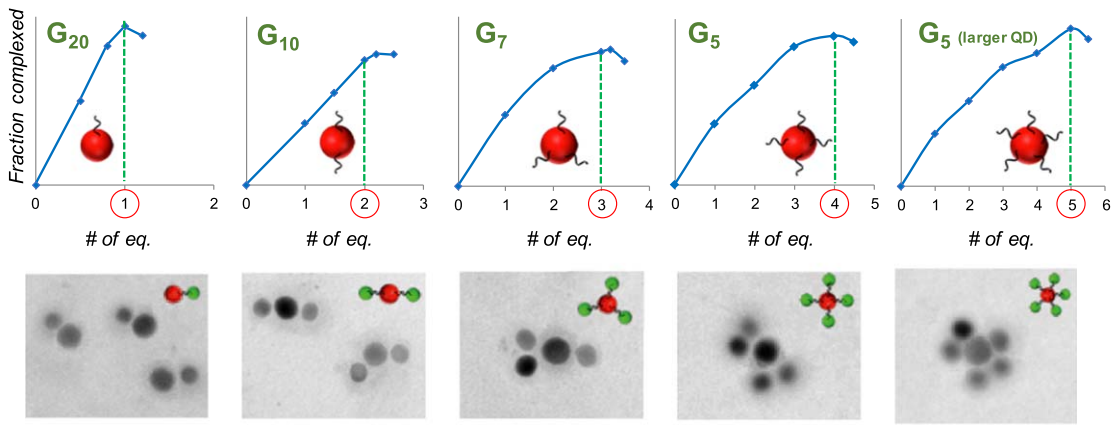

Figure 16. (**top**) Size exclusion chromatography results of DNA/QD conjugates synthesized with differently sized phosphorothiote domains and titrated with complementary sequences. (**bottom**) The degree of control over valency is shown through TEM images of QDs functionalized with 1–5 DNA strands and complexed with a second QD containing its complement. Reprinted with permission from [165]. Copyright 2011 Springer Nature.

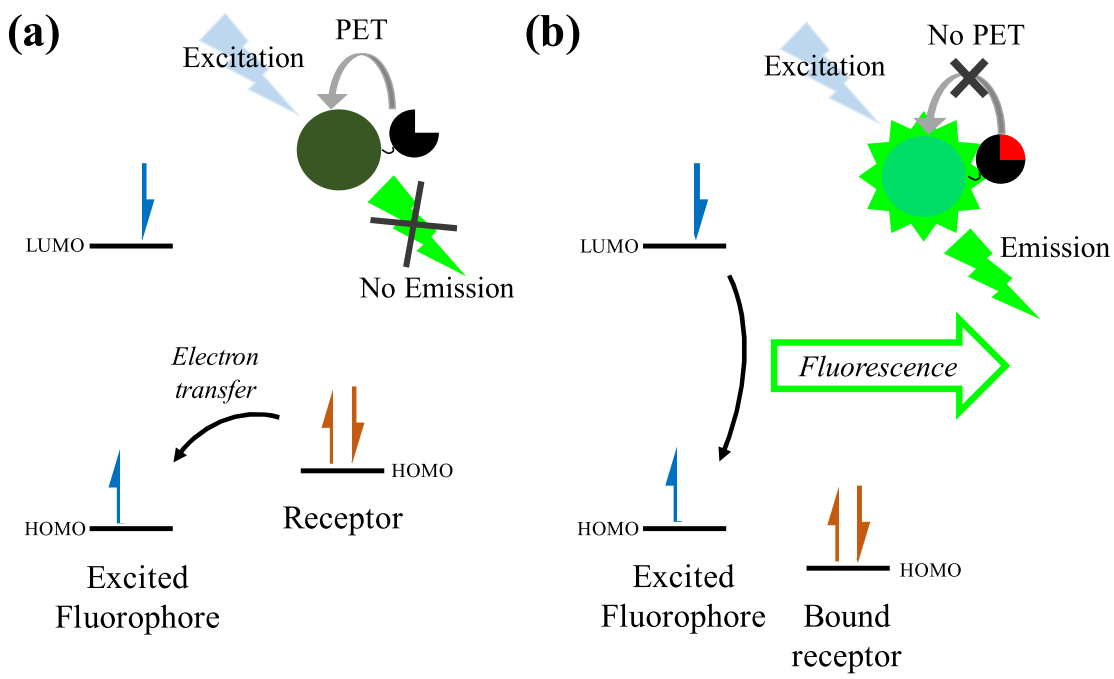

Figure 17. A schematic of using PET in sensing applications. (**a**) The receptor reduces the ground state of the fluorophore, preventing fluorescence. (**b**) In the presence of the sensor analyte, the receptor is bound and its HOMO is lowered, preventing PET from occurring and allowing fluorescence. This is an example of a 'turn on' sensor.

Mattera *et al* [149], to further improve the sensitivity of their immunoassay for PSA detection. IgGs and Fabs against PSA via their endogenous thiols within the antibodies (fragments) were directly conjugated to the surface of the Zn-rich QD surface (figure 14). This new and simple conjugation strategy allowed for an even more compact biosensor which allowed better LODs with 0.21 ng/mL for QDs conjugated to IgGs and 0.08 ng/mL for QDs conjugated to Fabs. As a comparison, the LOD for this QD-Fab was 10 and 25 times lower compared to conjugation via maleimide-terminated ligands [149] and polymer-coated QDs [148], respectively.

The work of Qiu *et al* demonstrated the necessity of careful QD-antibody conjugation optimization when taking into account antibody size, orientation, conjugation ratio and biological crosstalk on the performance of single and duplexed immunoassays [156]. By using different types of antibodies and orientations of nanobodies against EGFR and HER2, they obtained many combinations of QD-antibody/QD-nanobody + L4Tb-antibody/L4Tb-nanobody and tested each in a FRET immunoassay. Their findings showed that for a single assay, the highest sensitivity of EGFR was achieved using full-sized antibodies of cetuximab conjugated to L4Tb and matuzumab F(ab) on

eQD650, yielding an LOD of 2.9 ng mL^{-1}. An LOD of 8.0 ng mL^{-1} was determined for HER2 detection when using oriented nanobodies conjugated via their terminal cysteine to L4Tb and eQD605. As compared to using dyes for multiplexing [157], their duplexed immunoassay showed specific and sensitive detection of EGFR and HER2 from a single sample at low nanomolar concentrations without requiring complex spectral or biological correction [156]. With the same goal of improving QD-based immunoassays, Annio *et al* showed the importance of antibody-to-QD ratio in an FRET assay performance. They observed an 8-fold enhancement in LOD and 5-fold in the dynamic range of their FRET assay when increasing the number of IgG antibodies against total prostate specific antigen (TPSA) on the surface of QDs [22].

Díaz *et al* took advantage of the lanthanide-QD FRET system for kinetic studies by designing the first broad nanoparticle-based time-resolved FRET assay for adenosine diphosphate (ADP) [21]. In their sensor, QDs were labelled with a His6-ADP and antibodies recognizing ADP with a terbium complex (figure 15). Using a competitive assay format and a ratiometric measurement of the QD emission to terbium emission, they obtained a limit of detection of 10 nM ADP and a quantitation limit of 35 nM in a 20 μL sample volume using an 8 nM sensor concentration. Their sensor was further tested in an enzyme assay of glucokinase (GLK) and showed the ability to differentiate structurally similar enzyme inhibitors. Increasing concentrations of GLK favored faster reaction rates, and kinetic parameters could be determined from their experiments yielding a specificity constant of $210 \pm 100\ mM^{-1}\ s^{-1}$, $k_{cat}^{app} = 19 \pm 6\ s^{-1}$ and $k_M^{app} = 0.09 \pm 0.03$ mM. The inhibitory constant (K_i) for the coenzyme palmityl-CoA was determined to be $1.0 \pm 0.2\ \mu M$ in their buffer conditions, compared to a reported K_i of 2 μM in literature [21].

Upconverting nanoparticles (UCNPs) doped with lanthanide ions are uniquely able to emit UV/visible/NIR light following excitation with a NIR laser [158]. Since they can be excited in the NIR region, direct excitation of QDs is avoided with minimum background autofluorescence from biological samples. Doughan *et al* developed a paper-based FRET nucleic acid hybridization assay for the multiplexed detection of three oligonucleotides (ssDNA), namely uidA, Stx1A, and tetA, which are potential makers for the detection of *E. coli*. Core/shell UCNPs doped with Tm^{3+} and Yb^{3+} were immobilized on a paper substrate and conjugated to ssDNA, which was complementary to one part of the target ssDNA. Formation of UCNP-QD FRET pairs occurred when solutions containing QD-ssDNA and target DNA were added to the paper substrate. Upon NIR excitation, Tm^{3+} transferred non-radiative energy to the QDs and QD PL was observed due to FRET. The paper-based FRET sensor simultaneously detected uidA, Stx1A, and tetA with femtomole detection limits in both buffer and buffer containing 10% goat serum [159]. In a steady-state homogeneous FRET assay, Mattsson *et al* used UCNP-streptavidin-biotin-QD recognition as a biological model system. Upon 980 nm excitation of their UCNP doped with Er^{3+} and Yb^{3+}, their model system enabled the quantification of biotin in a competitive replacement assay through the sensitized emission of QD at 605 nm. Sensitized emission of the QD could be detected due to FRET from Er^{3+} ions to QDs but was relatively low in intensity due to the relatively large distance between Er^{3+} donors and QD acceptors as well as the low PL quantum yields of the UCNPs. Low nanomolar detection limits of biotin were still achievable, however, due to lack of sample autofluorescence and elimination of direct excitation of the QDs [160].

5.3. Quantum dot to quantum dot FRET

In QD-dye or QD-FP systems, the more photosensitive component is not directly excited, increasing the photostability of the system as a whole [132]. This can be further improved by completely ridding the system of photosensitive components by using a QDs as both the donor and acceptor. This could be advantageous for continuous sensing applications that require high stability and repeatability over many measurements. However, by using a quantum dot as an acceptor, the benefit of exciting only the donor molecule in QD-FP FRET is lost. In fact, because the energy at which a QD emits is inversely proportional to its size, in traditional QD-QD FRET systems the acceptor is larger than the donor, and therefore absorbs more of the excitation energy (figure 10(d)). This results in overwhelming acceptor background emission even in the absence of FRET. The high background can be alleviated by using an excess of donors, but at the cost of FRET efficiency. Intuitively, this makes sense, because the number of energy acceptors per energy donor is decreased, resulting in an overall decrease in energy transfer. The relationship between FRET efficiency and number of acceptors per donor (n) can be described mathematically by [31]:

$$E_{FRET} = \frac{nR_0{}^6}{nR_0{}^6 + r_{DA}{}^6} \tag{8}$$

Depending on the method of attaching acceptors to donors, the distribution of acceptors per donor within an ensemble can be modeled. For example, Pons *et al* showed through single particle measurements that fluorophores self-assembled through histidine binding to the QD metal ion surface formed subpopulations with different donor-acceptor ratios that could be modeled with a Poissonian distribution [161]. The advantages and pitfalls of QD-QD FRET are discussed in a comprehensive review published by Chou *et al* in 2015 [41], so only a few additional examples are described here.

One difficulty with engineering QD-QD FRET systems is controlling donor-acceptor ratios in

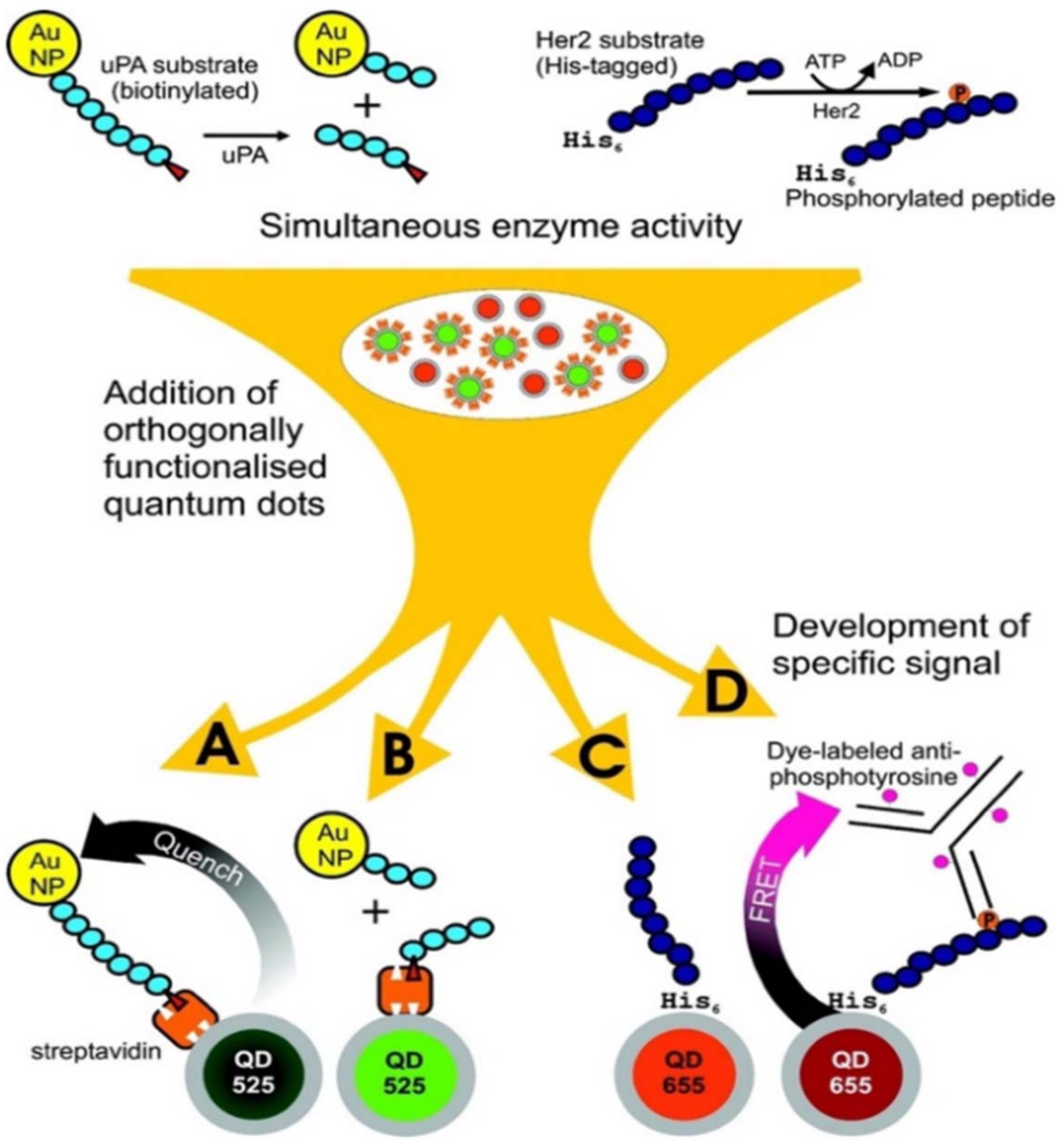

Figure 18. A schematic of a uPA protease and Her2 kinase multiplexed sensor. A biotinylated peptide labeled with a gold nanoparticle (AuNP) is susceptible to uPA cleavage, while a his-tagged Her2 substrate can be phosphorylated by Her2 in the presence of cofactor ATP. After enzyme activity, streptavidin-coated green QDs and MPA-coated red QDs are added to the mixture; the green QDs can bind the biotinylated peptides, while the Her2 substrate peptides peptides bind the red QDs as their small molecule ligand coating leaves the QD surface accessible for his-tag-mediated self-assembly. In the absence of uPA, the green QD is quenched by the AuNP; Her2 kinase activity phosphorylates the his-tagged peptide for further binding with dye-labeled anti-phosphotyrosine, enabling QD-dye FRET. Reprinted with permission from [138]. Copyright 2012 American Chemical Society.

the final QD-QD construct. Some functionalization schemes and strategies for creating monovalent DNA-QD conjugates have been explored [162, 163], but few have further extended their studies for control of multivalent systems. The most successful studies done to control the valency of DNA-QD conjugates use a one-step DNA-templated QD synthesis in aqueous solution where DNA strands containing phosphorothiote (ps) domains are present [164]. For example, in 2011 Tikhomirov *et al* published a report showing that the number of DNA strands per QD could be controlled by changing the length of the ps domain or size of the QD (figure 16) [165]. The authors showed that they were able to precisely control the valency of their QD-QD conjugates and demonstrated their use as sensors for pH and DNase. In the case of the pH sensor, the QDs exhibited differing degrees of QD-QD repulsion at different pH depending on the degree of deprotonation of their stabilizing ligands (MPA). At high pH, MPA is deprotonated and negatively charged and the QDs experienced interparticle charge repulsion, resulting in less energy transfer. At more neutral pH, the QDs were less charged and therefore experienced less repulsion. This resulted in an increase in energy transfer as a result of decreased distance between donor and acceptor QDs. The sensor was reversible (shown up to 5 cycles) indicating the robustness of the QD-DNA bond.

While the one-step aqueous synthesis scheme has yielded excellent results, the types of QDs that can be made is limited. To our knowledge, a heavy-metal free version of this scheme has yet to be reported. Reports of valence-controlled QDs synthesized in organic solvents by post modification have not seemed to be as successful. In 2015, Coopersmith *et al* [166] developed a method towards controlling the stoichiometry of QD-QD conjugates through a stepwise DNA-mediated assembly. By changing the ratio of acceptor to donor QDs during DNA hybridization, the authors demonstrated control of acceptor to donor ratios from 0–1.3. Perfectly uniform donor-acceptor ratios were not achieved, but the approach demonstrated a concerted means of improving the ratios, especially for small constructs, over standard solution-phase mixing. The development of a clean and efficient method of controlling acceptor to donor ratios is of interest for any who hope to use QDs in solution-phase sensing applications.

In a recent example, QD-QD FRET between [167] green and red In(Zn)P quantum dots was demonstrated with samples exhibiting QYs of up to 87%. The QDs were loaded into PMMA films at different donor to acceptor ratios. Lifetime measurements of the donor emission channel indicate FRET efficiency of up to 70% at the highest acceptor to donor ratio. PL analysis showed an increase in acceptor PL due to FRET, but also significant non-sensitized acceptor emission as expected in a QD-QD FRET system. This system was not used in a sensing application, but the development of bright, non-toxic QDs for use in QD-QD FRET is significant. Besides the obvious benefit of using non-toxic components, increasing the donor quantum yield in a FRET system also increases its FRET efficiency (equations (4*a*) and (5)).

6. Quantum dots in other types of energy transfer

6.1. Charge or electron transfer

QDs can extrinsically sense protons, metal ions, and other analytes through photoelectron transfer (PET) to a ligand on the surface. PET has been widely used in other fluorophores to sense many ions [168, 169], and QD PET has been studied both mechanistically [170, 171] and functionally [172–174]. Generally, PET-based sensors link a fluorophore to a receptor molecule with a highest occupied molecular orbital (HOMO) or lowest unoccupied molecular orbital (LUMO) that is higher than the fluorophore HOMO and lower than the fluorophore LUMO. Under these conditions, electron transfer between the receptor and the fluorophore occurs, quenching fluorescence (figure 17(a)) [175]. To utilize PET as a sensor, the receptor molecule has a functional group (*e.g.*, crown ether, tertiary amine, etc.) that binds ions or analytes, lowering the HOMO energy state of the receptor below the HOMO of the fluorophore (*i.e.*, raising the oxidative potential of the receptor). This prevents PET, turning on fluorescence (figure 17(b)).

The modularity of this approach has enabled the design of many ion sensors. In one of earliest papers using PET with QDs, Mulrooney *et al* linked a ferrocene urea moiety (which can bind fluorine anions) to the lipoic acid used for ligand exchange on CdSe/ZnS QDs [176]. The authors demonstrated a 25-fold increase in fluorescence after titrating to 200 mM fluorine. Furthermore, they showed that the addition of fluorine to a solution of their ligand caused a significant downward shift in the proton NMR of the urea group. This indicated that fluorescence quenching was caused by electron transfer from the lone pair on the nitrogen to the QD during excitation, while the fluorine ion changes the reduction potential of the lone pair and prevents transfer, thus turning on fluorescence.

PET based sensing is not limited to ions; electronic fields also impact electron transfer, inspiring the design of voltage sensors for biological imaging. In a more recent work by the Delehanty lab, a PET-based voltage sensor was designed by linking fullerenes to QDs with a membrane-inserting peptide [177]. The fullerene hydrophobicity paired with the membrane inserting peptide allowed for QDs to be distributed across cell surfaces with the peptides inserted in the membrane, while fullerenes act as an electron acceptor. At resting state in the neuron (−70 mV), the positive charge on the outside of the membrane prevented electron transfer, allowing bright fluorescence to occur. During cellular depolarization, the flipping of the field promoted electron transfer to the fullerenes. This yielded a 'turn off' sensor that outperformed standard voltage sensitive dyes in voltage sensitivity. This PET-based sensor also exhibited improved voltage sensing compared to the QCSE-based QD systems described above.

6.2. Nanometal surface energy transfer

Energy transfer between a QD and AuNP results in quenching of QD emission due to nanometal surface energy transfer (NSET), which is distance dependent to the inverse 4th power [178]. QD-AuNP systems have garnered interest due to their extended size range for sensing compared to FRET [179, 180]. Not only is energy transfer distance dependent to the inverse 4th power rather than inverse 6th, but the distance between the AuNP and QD is measured from the surface of the AuNP rather than the center. The size of the AuNP, therefore, does not contribute to the distance between the donor and acceptor, allowing for more flexibility when choosing the appropriate AuNP quencher. Very recently, Chen *et al* [181] confirmed this by calculating energy-transfer efficiencies from Tb donors bound to AuNP acceptors using the streptavidin-biotin interaction. They saw that changing the

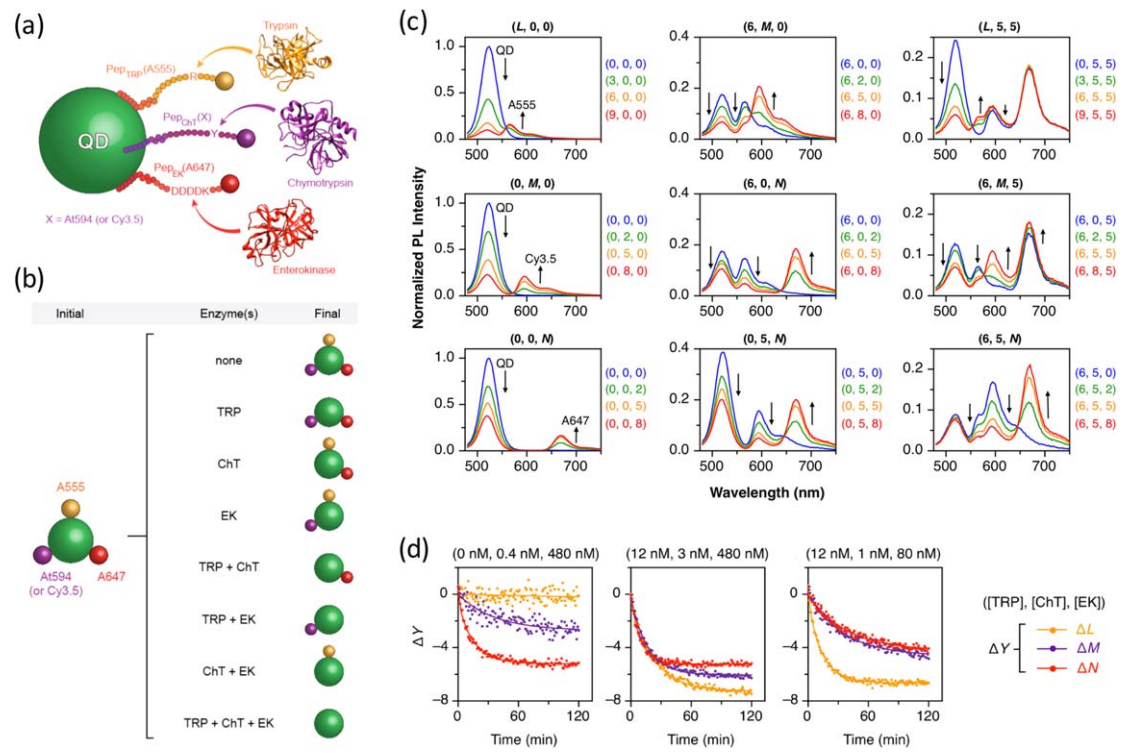

Figure 19. (**a**) Schematic of the donor QD labeled with three different peptide dye acceptors. (**b**) The resulting final QD-dye configurations of the multiplexed enzyme sensor with the addition of one, two, or all three of the analytes to be detected. (**c**) Titrations of the single (left), double (middle) and triple (right) acceptor systems. Numbers in position L, M, and N indicate the molar ratios of A555, Cy3.5, and A647 respectively to the QD donor. By analyzing the one acceptor system, behavior of the two acceptor system could be predicted and then further used to predict how the behavior of three acceptor systems. (d) Change in A555, Cy3.5, and A647 fluorescence intensity with the addition of different amounts of trypsin, chymotrypsin, and enterokinase, indicating the possibility of triply multiplexed biosensing using a single QD donor and multiple dye acceptors. Adapted with permission from [28]. Copyright 2017 American Chemical Society. Permission to further reproduce this material in any way should be directed to ACS for citation of the original article: https://pubs.acs.org/doi/abs/10.1021%2Facs.jpcc.7b02739.

AuNP size did not change the efficiency of energy transfer indicating that the quenching mechanism of PL lifetime of the donor by AuNPs were NSET rather than FRET-based.

Several examples of AuNP-mediated QD quenching used for sensing applications have been reported [182–187], but many difficulties still arise when trying to accurately predict how a NSET sensor will behave *a priori*. For example, Griffin *et al*, in a AuNP-dye sensor for RNA sensing, showed that when using 8 nm AuNPs, sensor quenching efficiency matched well with the theoretical model, while sensors using 40 nm and 70 nm AuNPs deviated significantly [188]. Using QDs and 30 nm AuNPs attached to triangular-shaped DNA origami, Samanta *et al* found that energy transfer was distance dependent to the inverse 2.7th, rather than 4th, power [189]. One possibility for the discrepancy discussed was the fact that the distance between the QDs and AuNPs as determined by TEM imaging could differ in solution phase, as the heavy AuNPs could cause slight bending in the DNA origami structure. The authors also specifically noted that the complexity of energy states present in QDs could be a contributing factor and that further investigation towards understanding the deviation from the NSET model is needed.

Another confounding factor when using AuNPs as quenchers is their overwhelmingly large molar extinction coefficients. While increased molar extinction coefficient results in increased spectral overlap, a severe increase in non-sensitized background quenching is also seen. By designing a DNA-linked AuNP-QD assembly that could dissociate in the presence of a DNA strand, the Maye group quantified the inner filter effect, finding that QD emission was quenched by over 50% even when using ~2x excess QDs per AuNPs [190]. Even so, their sensor exhibited ~20% recovery in PL intensity after the addition of the complex-breaking DNA.

In 2015, a more detailed study of AuNP-QD complexes evaluated how AuNP size and [AuNP]:[QD] ratio affect quenching efficiency [191]. Configurations comprising a single AuNP acceptor bound to multiple QD donors or *vice versa* were both tested. By studying the quenching efficiency and re-brightening in the presence of DNA, the authors found an optimal sensor design using a medium sized AuNP (13 nm) and an excess of 15 QDs per AuNP. This was found to be

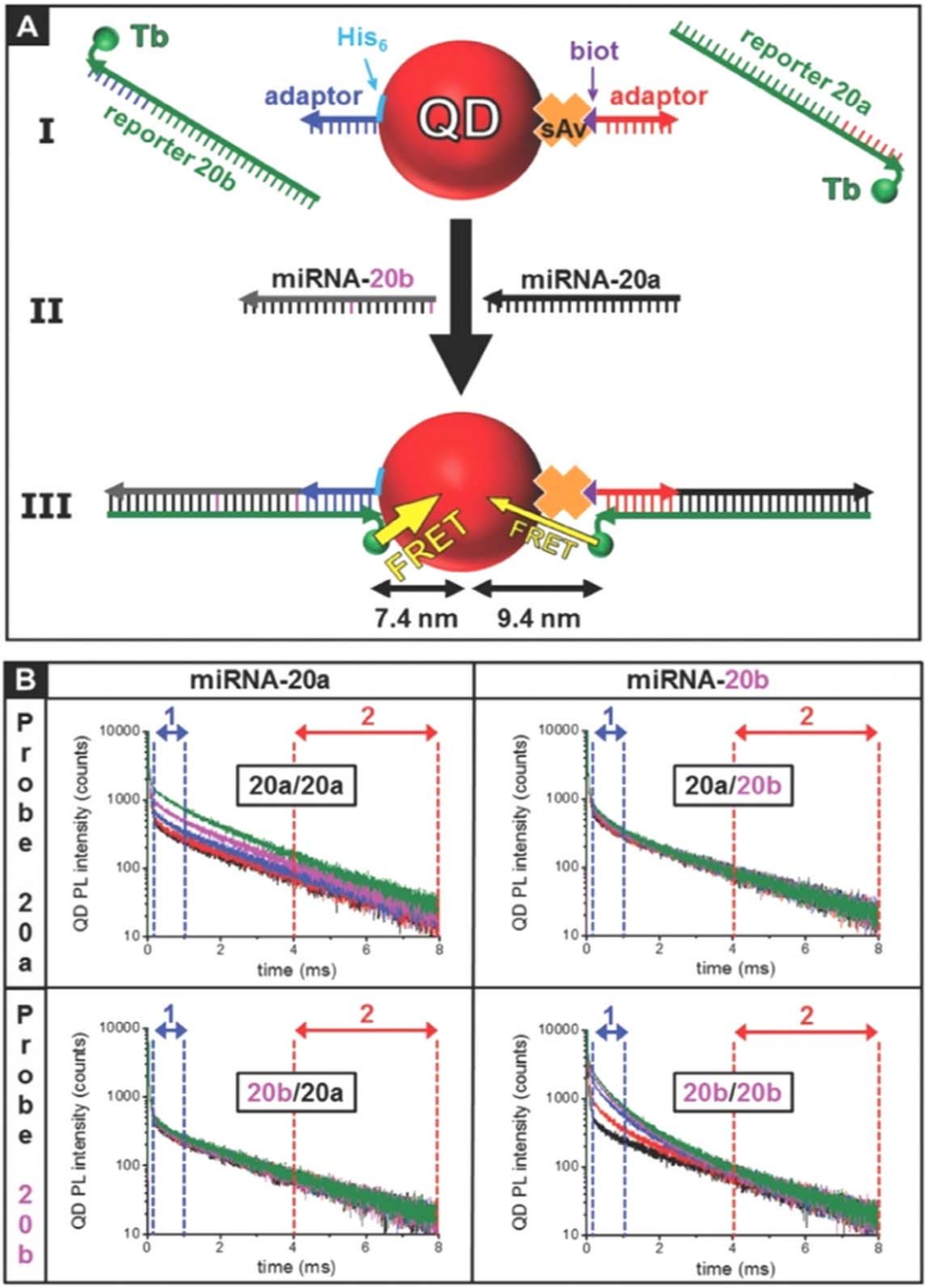

Figure 20. (**a**) Schematic of a multiplexed sensor using a single Tb-QD FRET pair that varies in donor-acceptor distance, and thus FRET efficiency, for each analyte of interest. (**b**) Lifetime measurements used for calibration of the multiplexed sensor. Adaptor sequences of the same length but bound to the QD through different conjugation means create different donor-acceptor separations for each Tb-QD energy pathway. By integrating fluorescence intensity in different time channels (**1** and **2**) and mathematically solving for equation (9), the concentration of two different miRNA strands can be detected simultaneously. Reprinted with permission from [24]. Copyright 2017, John Wiley and Sons.

optimal in terms of the overall brightness of the conjugate, while also exhibiting a significant change in PL intensity in the presence of target analyte. In addition to a fluorimeter, imaging and quantification was also performed with an iPad camera, demonstrating the feasibility of fluorescence detection using a consumer device. In addition, the author's attention to understanding the hybridization efficiency of AuNP/QD

conjugates gave insight on how steric hinderance impacts AuNP-QD sensor design, specifically when selecting the size of AuNPs and choosing donor acceptor ratios.

7. Multiplexed sensing

The ease of histidine-based self-assembly approaches described above combines well with the large surface area of the QD platform to facilitate the design and fabrication of multiplexed sensing systems. In the simplest case, multiple sensors using discretely colored donor QDs and acceptor fluorophores can be interrogated simultaneously using the spectrally distinct emission patterns following UV excitation [7, 138].

In 2012, Lowe *et al* [138] developed a sensor for simultaneous detection of uro-kinase-type plasminogen activator (uPA) protease activity and human epidermal growth factor receptor 2 (Her2) kinase activity. The simultaneous detection of both is of interest because the combination of uPA and Her2 biomarker concentrations can provide prognostic information for breast cancer patients. The key to their sensor design was simultaneous enzyme activity on the reactive peptides followed by the selective binding of each peptide/acceptor to its respective QD. For uPA sensing, an AuNP-labeled, biotinylated peptide was susceptible to cleavage by uPA. Likewise, a his-tagged peptide comprising the Her2 substrate could be phosphorylated at its target tyrosine residue by Her2, a change that could be discerned by the binding (or lack thereof) of a dye-labeled antiphosphotyrosine (an antibody specific for phosphorylated tyrosine). Streptavidin-coated QD525s and MPA-capped QD655s were bound by the biotinylated and his-tagged peptides, resulting in NSET or FRET, respectively, to an extent dependent on the corresponding enzyme activity (figure 18). As QD525 was quenched when the AuNPs were bound, QD525 brightness correlated to uPA activity. QD655 acted as a FRET donor to the AlexaFluor660-labeled antibody, and the ratio of fluorescence intensity at 655 and 660 indicated Her2 activity. The detection limit of uPA was 50 ng ml^{-1}, 10-fold improved from a previously reported bioluminescence resonance energy transfer (BRET) sensor, and 7.5 nM for Her2, which is comparable to previously published sensors. The success of this study highlights the advantages of using QDs in fluorescent sensors. Multiplexing with two colors was demonstrated, and low limits of detection were achieved due to the high degree of donor-acceptor labeling only possible when conjugating to a nanoparticle surface.

In 2015, Brazhnik *et al* [192] developed a quantum dot-based lab-on-a-bead system for multiplexed detection of different prostate cancer biomarkers. QDs were incorporated into microbeads functionalized with capture monoclonal antibodies (mAb) targeting specific antigens of interest. Detector antibodies were labeled with a secondary dye acting as a QD-FRET acceptor. Green and red QDs were used to monitor different antigens and flow cytometry used to analyze the tri-color QD/bead/dye system for simultaneous detection of free and total prostate-specific antigens. The study was performed using human serum samples and a clear discrimination between healthy and cancer patients was achieved. The sensor yielded similar results to single-analyte ELISAs, confirming the accuracy of the method—with the advantage of simultaneous detection. Furthermore, in this system no hook (or prozone) effect was observed. The hook effect is a false negative result that occurs in immunoassays when the antigen concentration saturates the antibody binding sites. Although this assay still used antibodies, implying that the Hook effect could eventually become a concern, the authors tested their system at antigen concentrations 4 to 5 times higher than standard concentration thresholds with no observable hook effect.

More evolved designs go beyond simply combining multiple existing sensors. For example, Algar *et al* [34] conjugated two different dye-labeled peptides to a central QD. The QD exhibited significant spectral overlap with one of the dyes, while the second dye aligned well as an acceptor to the first dye. This concentric relay design (cFRET) was used for multiplexed protease sensing [34]. While the attachment schemes for these systems are relatively simple, analysis can become difficult because the dyes can interact with each other as well as the quantum dot [28, 193]. In 2017, a three-acceptor cFRET system was demonstrated by attaching three different enzyme cleavable peptides labeled with three discrete dyes to a QD donor [28]. The energy transfer in a one-acceptor, two-acceptor, and three-acceptor system were systematically compared. It was found that PL quenching of a two-acceptor system can be predicted from the results of the one-acceptor configurations of its parts, and the two-acceptor system can likewise be used to predict the three-acceptor system—the general conclusion being that the system is found to behave effectively as a sum of its parts (figure 19).

Similarly, different energy transfer pathways can be combined for multiplexing. Algar *et al* [27] labeled DHLA- and DHLA-PEG-coated QDs with both a dye and ruthenium. Energy transfer to the dye is FRET-based, while energy transfer to the ruthenium is charge transfer (CT) based. CT results in decrease of only QD emission, while FRET results in both loss of QD emission as well as enhancement of dye emission. The molar ratio of QD:dye:Ru was varied and the effect on changes in PL studied. Because FRET and CT quench QD emission as a function of acceptor concentration at different rates, they were able to perform a multiplexed assay by first making calibration curves of QD:dye only and QD:Ru only complexes.

In the sensors described above, differences in spectral output is used for multiplexing. Lanthanide ions

are particularly useful in these designs, as they exhibit multiple narrow emission lines; by choosing QDs with emission peaks between or beyond the lanthanide peaks, multiplexed sensing of several biomarkers in a single sample can be achieved with minimal optical crosstalk [35–37]. In a clever alternative approach, Qiu *et al* [24] showed that time resolved FRET (TR-FRET) sensors using Tb-QD FRET can also be distinguished, and thus multiplexed, with careful analysis of the time-gated signal (figure 20). Two different micro-ribonucleic acid (miRNA) strands of the same length were conjugated to a QD surface either via biotin-streptavidin interaction or histidine self-assembly; these two conjugation approaches yield significantly different distances between the oligonucleotides and the QD. As a result, when Tb-labeled reporter strands bound to the QD in the presence of a specific miRNA sequence, the distance between the Tb donor and the QD acceptor depended on the conjugation approach, which was specific to the adapter/linker sequence. Because streptavidin is a large protein, Tb reporter sequences bound to the strep adaptor exhibited lesser FRET efficiency due to a larger donor-acceptor distance. By measuring the fluorescence lifetime of the sensor and correlating the PL intensity in different time windows, the concentrations of each miRNA strand could be calculated by solving the following set of equations:

$$\begin{bmatrix} S_1 \\ \vdots \\ S_n \end{bmatrix} = \begin{bmatrix} c_1 \\ \vdots \\ c_x \end{bmatrix} * \begin{bmatrix} z_1^1 & \cdots & z_x^1 \\ \vdots & \ddots & \vdots \\ z_1^n & \cdots & z_x^n \end{bmatrix} \tag{9}$$

where S_n is the background-subtracted PL intensity measured in time gate detection window, c_x is the concentration of analyte x, and z_x^n are the slopes of the calibration curves for each probe in each time window. The number of time windows measured and analyzed must equal the number of analytes probed to solve the system of equations. Through this strategy, single-step, multiplexed FRET assays with low nanomolar resolution were achieved. The same strategy has been recently applied to imaging [194]. Chen *et al* coated QDs with a 6 or 12 nm thiolated-silica shell before conjugating maleimide-functionalized terbium or europium (Eu) complexes to their surface. These four FRET NPs assembies (Tb-QD@SiO_2(6 nm), Tb-QD@SiO_2(12 nm), Eu-QD@SiO_2(6 nm) and Eu-QD@SiO_2(12 nm)) exhibited 4 distinct lifetimes of the QD acceptors. For each assembly, the acceptor lifetime was split into 3 different time-gated windows defined as red, green, or blue (RGB). The authors demonstrated multiplexing capabilities by encoding Hela cells with the four different FRET pairs separately and then mixing them on the same slide. Because each pair had a distinct RGB code generated through time gating of its QD lifetime, cells incubated with the different assemblies could be distinguished using a single emission filter [194].

8. Challenges and future prospects

QDs have been synthesized and studied for over 30 years, but have yet to be integrated into commercial biosensors despite their remarkable optical properties. One concern is toxicity [195–197]. Many of the QDs used in the previously discussed sensors included toxic materials, namely, cadmium. While the toxicity of Cd-based QDs is not a biocompatibility concern for *in vitro* sensors, there is still a general push in the field away from toxic constituents [198–201]. In this context, the use of Cd-free $CuInS_2$ QDs in a FLISA has been demonstrated [202].

While the development of cheap imaging methods for fluorescent assays hold a lot of promise for making QD-based POC devices commercially translatable, several issues can still be addressed—for example, improving the smart-phone camera's ability to resolve narrow emission bandwidths, as well as discern QD fluorescence from the autofluorescence of many paper-based substrates. A review was recently written by Ulep and Yoon describing these issues and the current technologies under examination for potentially alleviating them—for example, optimizing optical setups or developing digital enhancement algorithms [203].

Specifically, with immunoassays, Ab-functionalization of the QD surface is non-trivial. While several biofunctionalization methods exist, creating the optimal Ab-QD conjugate can be challenging. As previously mentioned, Ab affinity can decrease after attachment to a QD [7]. One reason for this is the difficulty of precisely orienting antibodies on the QD. It is imperative that the binding sites of the Abs are available to the surrounding environment and not facing the QD [156]. Another challenge in attachment chemistry is the colloidal nature of the QDs. QD conjugates should be stable in solution, but traditional covalent chemistries can increase the likelihood of QD aggregation, causing huge loses in product [48]. Other considerations that effect the function of Ab-QD conjugates include the type of linkage between the Ab and QD and the overall size of the conjugate [204–206]. Furthermore, the price of producing QD-based immunoassays becomes unnecessarily high when low reaction yields result in the waste of expensive monoclonal antibodies [60]. Oligo or peptide aptamers are much more economical, but finding sequences with comparable affinities to clinically relevant antibodies is a field of study that is still under development [207].

Advances in QD biofunctionalization have been made, with the most recent and promising being reagent-free and bio-orthogonal chemistries [48]. Reagent-free reactions do not require external coupling reagents and are free of byproducts, the classic example being the biotin-streptavidin interaction [24, 138]. In this case, the two moieties to be coupled and labeled with either biotin or streptavidin and

allowed to bind. More recent methods include thiol-maleimide coupling [208, 209] and disulfide formation [210, 211]. Bio-orthogonal chemistries are defined as reactions that can occur within biological systems without disrupting their function. Some examples include SNAP [212, 213] and HALO [214–216] tag techniques as well as copper-free click chemistry [154, 217, 218]. Further developing the chemistries to create high affinity, stable, and reproducible Ab-QDs will make the development of QD-based FLISAs for the commercial market more likely.

9. Conclusions

The development of QD-based fluorescent sensors is of interest because of the unique properties specific to QDs that can be used to improve currently existing sensor designs. QDs are bright and photostable with size-tunable, narrow, and symmetric emission profiles. The broadband absorption of QDs allows for multiple emitters to be excited with a single wavelength, enabling multiplexed systems with simplified analysis. Several different ligands and molecules can be bound to the QD metal-ion surface, increasing the modularity and flexibility of QD sensors. Examples of QD-based sensors that obtain the same or improved abilities of previously existing commercial assays or contemporary research tools have been shown, but so far, few have actually replaced their preexisting technologies. Despite being commercially available for over a decade, QDs are still expensive relative to common fluorescent dyes. The added concern over the toxicity of nanoparticles—specifically those comprised of heavy metals—further dissuades those not directly involved in QD research to use them. For this reason, further development of cost-effective, non-heavy metal-based QD synthesis is of utmost importance for eventually making the use of QDs in fluorescent sensors standard. Moreover, while a multitude of functionalization schemes exist, complete and precise control of the nanoparticle surface is still out of reach. Regardless, the superior optical properties and unique size regime that is larger than molecular, yet smaller than bulk, provide a niche of applications that can be greatly improved by the use of QDs.

Acknowledgments

This publication was supported by the National Center for Advancing Translational Sciences, National Institutes of Health, through BU-CTSI Grant Number 1KL2TR001411. Its contents are solely the responsibility of the authors and do not necessarily represent the official views of the NIH. Financial support for JCK provided by Training Grant NIH/NIGMS T32 GM008764. SB was funded by a postdoctoral fellowship from the Precision Diagnostics Center at Boston University.

ORCID iDs

Allison M Dennis https://orcid.org/0000-0001-5759-9905

References

[1] Demchenko A P 2015 Fluorescence Detection Techniques *Introduction to Fluorescence Sensing* 2 (Switzerland: Springer International Publishing) 3 pp 69–132978-3-319-20779-7
[2] Demchenko A P 2015 Molecular-Size Fluorescence Emitters *Introduction to Fluorescence Sensing* 2 (Switzerland: Springer International Publishing) 4 133–202978-3-319-20779-7
[3] Jayant K *et al* 2017 Targeted intracellular voltage recordings from dendritic spines using quantum-dot-coated nanopipettes *Nat. Nanotechnol.* **12** 335–42
[4] Lv Y, Wu R, Feng K, Li J, Mao Q, Yuan H, Shen H, Chai X and Li L S 2017 Highly sensitive and accurate detection of C-reactive protein by CdSe/ZnS quantum dot-based fluorescence-linked immunosorbent assay *J. Nanobiotechnology* **15** 35
[5] Zhu X, Chen L, Shen P, Jia J, Zhang D and Yang L 2011 High sensitive detection of Cry1Ab protein using a quantum dot-based fluorescence-linked immunosorbent assay *J. Agric. Food Chem.* **59** 2184–9
[6] Zhu K, Li J, Wang Z, Jiang H, Beier R C, Xu F, Shen J and Ding S 2011 Simultaneous detection of multiple chemical residues in milk using broad-specificity antibodies in a hybrid immunosorbent assay *Biosens. Bioelectron.* **26** 2716–9
[7] Peng C *et al* 2009 Simultaneous and sensitive determination of multiplex chemical residues based on multicolor quantum dot probes *Biosens. Bioelectron.* **24** 3657–62
[8] Choudhury D, Jaque D, Rodenas A, Ramsay W T, Paterson L and Kar A K 2012 Quantum dot enabled thermal imaging of optofluidic devices *Lab Chip* **12** 2414–20
[9] Bensalah K, Tuncel A, Hanson W, Stern J, Han B and Cadeddu J 2010 Monitoring of thermal dose during ablation therapy using quantum dot-mediated fluorescence thermometry *J. Endourol.* **24** 1903–8
[10] Tycko R 2014 Remote sensing of sample temperatures in nuclear magnetic resonance using photoluminescence of semiconductor quantum dots *J. Magn. Reson.* **244** 64–7
[11] Kameya T, Matsuda Y, Egami Y, Yamaguchi H and Niimi T 2014 Dual luminescent arrays sensor fabricated by inkjet-printing of pressure- and temperature-sensitive paints *Sens. Actuators B Chem.* **190** 70–7
[12] Liu W *et al* 2014 Planar temperature sensing using heavy-metal-free quantum dots with micrometer resolution *Nanotechnology* **25** 285501
[13] Chen Y F and Rosenzweig Z 2002 Luminescent CdS quantum dots as selective ion probes *Anal. Chem.* **74** 5132–8
[14] Luo X B, Guo B, Wang L C, Deng F, Qi R X, Luo S L and Au C T 2014 Synthesis of magnetic ion-imprinted fluorescent CdTe quantum dots by chemical etching and their visualization application for selective removal of Cd(II) from water *Colloids Surf.* A **462** 186–93
[15] Mu Q, Li Y, Xu H, Ma Y, Zhu W and Zhong X 2014 Quantum dots-based ratiometric fluorescence probe for mercuric ions in biological fluids *Talanta* **119** 564–71
[16] Wang J, Jiang C, Wang X, Wang L, Chen A, Hu J and Luo Z 2016 Fabrication of an 'ion-imprinting' dual-emission quantum dot nanohybrid for selective fluorescence turn-on and ratiometric detection of cadmium ions *Analyst* **141** 5886–92
[17] Wu P and Yan X P 2010 A simple chemical etching strategy to generate 'ion-imprinted' sites on the surface of quantum dots for selective fluorescence turn-on detecting of metal ions *Chem. Commun.* **46** 7046–8
[18] Park K *et al* 2018 Membrane insertion of-and membrane potential sensing by-semiconductor voltage nanosensors: feasibility demonstration *Sci. Adv.* **4** e1601453

[19] Hsia C H, Wuttig A and Yang H 2011 An accessible approach to preparing water-soluble Mn^{2+}-doped (CdSSe)ZnS (core) shell nanocrystals for ratiometric temperature sensing *ACS Nano* **5** 9511–22
[20] Huang G G, Wang C L, Xu X J and Cui Y P 2016 An optical ratiometric temperature sensor based on dopant-dependent thermal equilibrium in dual-emitting Ag&Mn:ZnInS quantum dots *RSC Adv.* **6** 58113–7
[21] Díaz S A, Lasarte-Aragones G, Lowery R G, Aniket, Vranish J N, Klein W P, Susumu K and Medintz I L 2018 Quantum dots as förster resonance energy transfer acceptors of lanthanides in time-resolved bioassays *ACS Appl. Nano Mater.* **1** 3006–14
[22] Annio G, Jennings T L, Tagit O and Hildebrandt N 2018 Sensitivity enhancement of forster resonance energy transfer immunoassays by multiple antibody conjugation on quantum dots *Bioconjug. Chem.* **29** 2082–9
[23] Massey M, Li J J and Algar W R 2017 Multifunctional Concentric FRET-Quantum Dot Probes for Tracking and Imaging of Proteolytic Activity. *Cancer Nanotechnology Methods and Protocols* (*Methods in Molecular Biology* 1530) (New York, NY: Humana Press) 63–97 978-1-4939-6646-2
[24] Qiu X, Guo J, Jin Z, Petreto A, Medintz I L and Hildebrandt N 2017 Multiplexed nucleic acid hybridization assays using single-FRET-pair distance-tuning *Small* **13** 1700332
[25] Chern M, Nguyen T T, Mahler A H and Dennis A M 2017 Shell thickness effects on quantum dot brightness and energy transfer *Nanoscale* **9** 16446–58
[26] Hildebrandt N, Spillmann C M, Algar W R, Pons T, Stewart M H, Oh E, Susumu K, Diaz S A, Delehanty J B and Medintz I L 2017 Energy transfer with semiconductor quantum dot bioconjugates: a versatile platform for biosensing, energy harvesting, and other developing applications *Chem. Rev.* **117** 536–711
[27] Algar W R, Khachatrian A, Melinger J S, Huston A L, Stewart M H, Susumu K, Blanco-Canosa J B, Oh E, Dawson P E and Medintz I L 2017 Concurrent modulation of quantum dot photoluminescence using a combination of charge transfer and forster resonance energy transfer: competitive quenching and multiplexed biosensing modality *J. Am. Chem. Soc.* **139** 363–72
[28] Massey M, Kim H, Conroy E M and Algar W R 2017 Expanded quantum dot-based concentric forster resonance energy transfer: adding and characterizing energy-transfer pathways for triply multiplexed biosensing *J. Phys. Chem.* C **121** 13345–56
[29] Zwier J M and Hildebrandt N 2017 Time-Gated FRET Detection for Multiplexed Biosensing *Reviews in Fluorescence 2016* (*Reviews in Fluorescence*) (Cham: Springer) 17–43978-3-319-48260-6
[30] Shamirian A, Ghai A and Snee P T 2015 QD-based FRET probes at a glance *Sensors* **15** 13028–51
[31] Medintz I and Hildebrandt N 2014 *FRET — Förster resonance energy transfer: from theory to applications* (Weinhiem, Germany: Wiley-VCH) 9783527328161 (https://doi.org/10.1002/9783527656028)
[32] Banerjee A, Pons T, Lequeux N and Dubertret B 2016 Quantum dots-DNA bioconjugates: synthesis to applications *Interface Focus* **6** 20160064
[33] Medintz I L, Uyeda H T, Goldman E R and Mattoussi H 2005 Quantum dot bioconjugates for imaging, labelling and sensing *Nat. Mater.* **4** 435–46
[34] Algar W R, Ancona M G, Malanoski A P, Susumu K and Medintz I L 2012 Assembly of a concentric Forster resonance energy transfer relay on a quantum dot scaffold: characterization and application to multiplexed protease sensing *ACS Nano* **6** 11044–58
[35] Cardoso Dos Santos M and Hildebrandt N 2016 Recent developments in lanthanide-to-quantum dot FRET using time-gated fluorescence detection and photon upconversion *TrAC* **84** 60–71
[36] Sy M, Nonat A, Hildebrandt N and Charbonniere L J 2016 Lanthanide-based luminescence biolabelling *Chem. Commun.* **52** 5080–95
[37] Hildebrandt N and Geißler D 2011 Semiconductor Quantum Dots as FRET Acceptors for Multiplexed Diagnostics and Molecular Ruler Application *Nano-Biotechnology for Biomedical and Diagnostic Research* (*Advances in Experimental Medicine and Biology*) (Dordrecht: Springer) **733** 97–114978-94-007-2555-3
[38] Lindsay S 2010 *Introduction to Nanoscience* (Oxford: Oxford University Press) 0199544212
[39] O'Neil M, Marohn J and McLendon G 1990 Dynamics of electron-hole pair recombination in semiconductor clusters *J. Phys. Chem.* **94**
[40] Skolnick M S and Mowbray D J 2004 SELF-ASSEMBLED SEMICONDUCTOR QUANTUM DOTS: fundamental physics and device applications *Ann. Rev. of Mater. Res.* **34** 181–218
[41] Chou K F and Dennis A M 2015 Förster resonance energy transfer between quantum dot donors and quantum dot acceptors *Sensors* **15** 13288–325
[42] Manasreh O 2005 *Semiconductor Heterojunctions and Nanostructures* (New York, NY: McGraw-Hill) 9780071469685 (https://doi.org/10.1036/9780071469685)
[43] Güçlü A D 2014 *Graphene Quantum Dots* (*NanoScience and Technology*) (Berlin: Springer) 978-3-662-44611-9 (https://doi.org/10.1007/978-3-662-44611-9)
[44] Shiohara A, Hanada S, Prabakar S, Fujioka K, Lim T H, Yamamoto K, Northcote P T and Tilley R D 2010 Chemical reactions on surface molecules attached to silicon quantum dots *J. Am. Chem. Soc.* **132** 248–53
[45] Valeur B and Berberan-Santos M N 2013 *Molecular Fluorescence principles and applications* 2 (Weinheim: Wiley-VCH) https://ebookcentral.proquest.com/lib/bu/detail.action?docID=1161964 9783527650033
[46] Resch-Genger U, Grabolle M, Cavaliere-Jaricot S, Nitschke R and Nann T 2008 Quantum dots versus organic dyes as fluorescent labels *Nat. Methods* **5** 763–75
[47] Lim S J, Zahid M U, Le P, Ma L, Entenberg D, Harney A S, Condeelis J and Smith A M 2015 Brightness-equalized quantum dots *Nat. Commun.* **6** 8210
[48] Tyrakowski C M and Snee P T 2014 A primer on the synthesis, water-solubilization, and functionalization of quantum dots, their use as biological sensing agents, and present status *Phys. Chem. Chem. Phys.* **16** 837–55
[49] Bruno J G 2014 Application of DNA aptamers and Quantum dots to lateral flow test strips for detection of foodborne pathogens with improved sensitivity versus colloidal gold *Pathogens* **3** 341–55
[50] Enzyme Substrates for ELISA ThermoFisher Scientific (https://thermofisher.com/us/en/home/life-science/protein-biology/protein-assays-analysis/elisa/elisa-reagents-buffers/enzyme-substrates-elisa.html) 12 2018
[51] Goldman E R, Anderson G P, Tran P T, Mattoussi H, Charles P T and Mauro J M 2002 Conjugation of luminescent quantum dots with antibodies using an engineered adaptor protein to provide new reagents for fluoroimmunoassays *Anal. Chem.* **74** 841–7
[52] Medintz I L, Clapp A R, Mattoussi H, Goldman E R, Fisher B and Mauro J M 2003 Self-assembled nanoscale biosensors based on quantum dot FRET donors *Nat. Mater.* **2** 630–8
[53] Song E, Yu M, Wang Y, Hu W, Cheng D, Swihart M T and Song Y 2015 Multi-color quantum dot-based fluorescence immunoassay array for simultaneous visual detection of multiple antibiotic residues in milk *Biosens. Bioelectron.* **72** 320–5
[54] Luo Y, Zhang B, Chen M, Jiang T, Zhou D, Huang J and Fu W 2012 Sensitive and rapid quantification of C-reactive protein using quantum dot-labeled microplate immunoassay *J. Trans. Med.* **10** 24

[55] Petryayeva E and Algar W R 2015 Toward point-of-care diagnostics with consumer electronic devices: the expanding role of nanoparticles *RSC Adv.* **5** 22256–82
[56] Duchesne L and Lacombe K 2018 Innovative technologies for point-of-care testing of viral hepatitis in low-resource and decentralized settings *J. Viral. Hepat.* **25** 108–17
[57] Cheng S *et al* 2017 A new immunoassay of serum antibodies against peste des petits ruminants virus using quantum dots and a lateral-flow test strip *Anal. Bioanal. Chem.* **409** 133–41
[58] Wu F, Yuan H, Zhou C, Mao M, Liu Q, Shen H, Cen Y, Qin Z, Ma L and Song Li L 2016 Multiplexed detection of influenza A virus subtype H5 and H9 via quantum dot-based immunoassay *Biosens. Bioelectron.* **77** 464–70
[59] Wu R, Zhou S, Chen T, Li J, Shen H, Chai Y and Li L S 2018 Quantitative and rapid detection of C-reactive protein using quantum dot-based lateral flow test strip *Anal. Chim. Acta.* **1008** 1–7
[60] Qi X, Huang Y, Lin Z, Xu L and Yu H 2016 Dual-Quantum-dots-labeled lateral flow strip rapidly quantifies procalcitonin and C-reactive protein *Nanoscale Res. Lett.* **11** 167
[61] Li Z, Wang Y, Wang J, Tang Z, Pounds J G and Lin Y 2010 Rapid and sensitive detection of protein biomarker using a portable fluorescence biosensor based on quantum dots and a lateral flow test strip *Anal. Chem.* **82** 7008–14
[62] Liu J Z, Ji D Y, Meng H M, Zhang L, Wang J Y, Huang Z M, Chen J, Li J J and Li Z H 2018 A portable fluorescence biosensor for rapid and sensitive glutathione detection by using quantum dots-based lateral flow test strip *Sens. Actuators B Chem.* **262** 486–92
[63] Wang S, Liu Y, Jiao S, Zhao Y, Guo Y, Wang M and Zhu G 2017 Quantum-Dot-based lateral flow immunoassay for detection of neonicotinoid residues in tea leaves *J. Agric. Food Chem.* **65** 10107–14
[64] Karlen W and Iniewski K 2014 *Mobile point-of-care monitors and diagnostic device design* 1 (Boca Raton: CRC Press) https://www.crcpress.com/Mobile-Point-of-Care-Monitors-and-Diagnostic-Device-Design/Karlen/p/book/9781466589292
[65] Petryayeva E and Algar W R 2015 Single-step bioassays in serum and whole blood with a smartphone, quantum dots and paper-in-PDMS chips *Analyst* **140** 4037–45
[66] Zhu H, Sikora U and Ozcan A 2012 Quantum dot enabled detection of *Escherichia coli* using a cell-phone *Analyst* **137** 2541–4
[67] Petryayeva E and Algar W R 2014 Multiplexed homogeneous assays of proteolytic activity using a smartphone and quantum dots *Anal. Chem.* **86** 3195–202
[68] Petryayeva E and Algar W R 2016 A job for quantum dots: use of a smartphone and 3D-printed accessory for all-in-one excitation and imaging of photoluminescence *Anal. Bioanal. Chem.* **408** 2913–25
[69] Wang X D, Wolfbeis O S and Meier R J 2013 Luminescent probes and sensors for temperature *Chem. Soc. Rev.* **42** 7834–69
[70] Varshni Y P 1967 Temperature dependence of the energy gap in semiconductors *Physica* 34 (Elsevier) 149–54
[71] Biju V, Makita Y, Sonoda A, Yokoyama H, Baba Y and Ishikawa M 2005 Temperature-sensitive photoluminescence of CdSe quantum dot clusters *J. Phys. Chem.* B **109** 13899–905
[72] Kim J C, Rho H, Smith L M, Jackson H E, Lee S, Dobrowolska M and Furdyna J K 1999 Temperature-dependent micro-photoluminescence of individual CdSe self-assembled quantum dots *Appl. Phys. Lett.* **75** 214–6
[73] Morello G, De Giorgi M, Kudera S, Manna L, Cingolani R and Anni M 2007 Temperature and size dependence of nonradiative relaxation and exciton-phonon coupling in colloidal CdTe quantum dots *J. Phys. Chem. C* **111** 5846–9
[74] Wu Y H, Arai K and Yao T 1996 Temperature dependence of the photoluminescence of ZnSe/ZnS quantum-dot structures *Phys. Rev.* B **53** 10485–8
[75] Jagtap A M, Chatterjee A, Banerjee A, Pendyala N B and Rao K S R K 2016 Size and temperature dependence of the photoluminescence properties of NIR emitting ternary alloyed mercury cadmium telluride quantum dots *J. Phys. D: Appl. Phys.* **49** 135302
[76] Zhao W R, Weng G E, Liang M M, Li Z C, Liu J P, Zhang J Y and Zhang B P 2014 Temperature dependence of emission properties of self-assembled InGaN Quantum dots *Chinese Phys. Lett.* **31** 114205
[77] Keuleyan S, Kohler J and Guyot-Sionnest P 2014 Photoluminescence of Mid-Infrared HgTe colloidal quantum dots *J. Phys. Chem.* C **118** 2749–53
[78] Phadnis C, Sonawane K G, Sudarsan V and Mahamuni S 2017 The implications of grading on the emission line width of core–shell nanocrystals *J. Phys. D: Appl. Phys.* **50** 145302
[79] Pal U, Pérez J L H, Piqueras J and Dieguéz E 1996 Near band gap photoreflectance studies in CdTe, CdTe:V and CdTe:Ge crystals *Mater. Sci. Eng.* B **42** 297–301
[80] Harbord E, Iwamoto S, Arakawa Y, Spencer P, Clarke E and Murray R 2012 Influence of p-doping on the temperature dependence of InAs/GaAs quantum dot excited state radiative lifetime *Appl. Phys. Lett.* **101** 183108
[81] Turyanska L, Patane A, Henini M, Hennequin B and Thomas N R 2007 Temperature dependence of the photoluminescence emission from thiol-capped PbS quantum dots *Appl. Phys. Lett.* **90** 101913
[82] Jiang X B, Shao J Y and Li B Q 2017 Ceiling temperature and photothermalsensitivity of aqueous MSA-CdTe quantum dots thermometers *Appl. Surf. Sci.* **394** 554–61
[83] Walker G W, Sundar V C, Rudzinski C M, Wun A W, Bawendi M G and Nocera D G 2003 Quantum-dot optical temperature probes *Appl. Phys. Lett.* **83** 3555–7
[84] Valerini D, Cretí A, Lomascolo M, Manna L, Cingolani R and Anni M 2005 Temperature dependence of the photoluminescence properties of colloidal CdSe／ZnS core/shell quantum dots embedded in a polystyrene matrix *Phys. Rev.* B **71** 235409
[85] Chon B, Bang J, Park J, Jeong C, Choi J H, Lee J B, Joo T and Kim S 2011 Unique Temperature Dependence and Blinking Behavior of CdTe/CdSe (Core/Shell) Type-II Quantum Dots *J. Phys. Chem.* C **115** 436–42
[86] Reznitsky A, Klochikhin A and Permogorov S 2012 Temperature quenching of PL intensity and mechanisms of carrier recombination in CdTe/ZnTe self-assembled quantum dots *Phys. Status Solidi* C **9** 1624–6
[87] Wen Y C, Kuo H C, Guo J L and Jia H W 2016 Nuclear Magnetic Resonance Spectroscopy Investigation on Ultralow Melting Temperature Behavior of Dimethyl Sulfoxide-Water Solutions *J. Phys. Chem.* B **120** 13125–35
[88] Yamamoto K, Caporini M A, Im S, Waskell L and Ramamoorthy A 2013 Shortening spin-lattice relaxation using a copper-chelated lipid at low-temperatures - A magic angle spinning solid-state NMR study on a membrane-bound protein *J. Magn. Reson.* **237** 175–81
[89] Tycko R 2013 NMR at low and ultralow temperatures *Acc. Chem. Res.* **46** 1923–32
[90] Liu Q, Sleiti A K and Kapat J S 2008 Application of pressure and temperature sensitive paints for study of heat transfer to a circular impinging air jet *Int. J. Therm. Sci.* **47** 749–57
[91] Engler R H, Fey U, Henne U, Klein C and Sachs W E 2005 Quantitative wind tunnel studies using pressure- and temperature sensitive paints *J. Visualization* **8** 277–84
[92] Matsuda Y, Torimoto T, Kameya T, Kameyama T, Kuwabata S, Yamaguchi H and Niimi T 2013 ZnS-$AgInS_2$ nanoparticles as a temperature sensor *Sens. Actuators B Chem.* **176** 505–8
[93] Larrión B, Hernáez M, Arregui F J, Goicoechea J, Bravo J and Matías I R 2009 Photonic Crystal Fiber Temperature Sensor Based on Quantum Dot Nanocoatings *J. Sens.* **2009** 1–6
[94] Wang S, Dai Z, Ke H, Qu E, Qi X, Zhang K and Wang J 2014 Contrast ultrasound-guided photothermal therapy using gold nanoshelled microcapsules in breast cancer *Eur. J. Radiol.* **83** 117–22
[95] Crawford B M, Shammas R L, Fales A M, Brown D A, Hollenbeck S T, Vo-Dinh T and Devi G R 2017 Photothermal ablation of inflammatory breast cancer tumor emboli using plasmonic gold nanostars *Int. J. Nanomedicine* **12** 6259–72

[96] Liu Y *et al* 2015 A Plasmonic Gold Nanostar Theranostic Probe for *In Vivo* Tumor Imaging and Photothermal Therapy *Theranostics* **5** 946–60
[97] Bower S M, Kou J and Saylor J R 2009 A method for the temperature calibration of an infrared camera using water as a radiative source *Rev. Sci. Instrum.* **80** 095107
[98] Ding X, Qu L, Yang R, Zhou Y and Li J 2015 A highly selective and simple fluorescent sensor for mercury (II) ion detection based on cysteamine-capped CdTe quantum dots synthesized by the reflux method *Luminescence* **30** 465–71
[99] Mandal A, Dandapat A and De G 2012 Magic sized ZnS quantum dots as a highly sensitive and selective fluorescence sensor probe for Ag + ions *Analyst* **137** 765–72
[100] Wu D D, Chen Z, Huang G B and Liu X G 2014 ZnSe quantum dots based fluorescence sensors for Cu^{2+} ions *Sens. Actuators A Phys.* **205** 72–8
[101] Xing X W, Wang D M, Chen Z, Zheng B D, Li B H and Wu D D 2018 ZnTe quantum dots as fluorescence sensors for the detection of iron ions *J. Mater. Sci-Mater. EL.* **29** 14192–9
[102] Kamat P V 1993 Photochemistry on Nonreactive and Reactive (Semiconductor) Surfaces *Chem. Rev.* **93** 267–300
[103] Wang J, Jiang C X, Yang F, Chen A M, Wang L G and Hu J 2016 Controlled synthesis of a dual-emission hierarchical quantum dot hybrid nanostructure as a robust ratiometric fluorescent sensor *RSC Adv.* **6** 15716–23
[104] Miller D A B, Chemla D S, Damen T C, Gossard A C, Wiegmann W, Wood T H and Burrus C A 1984 Band-edge electroabsorption in quantum well structures: the quantum-confined stark-effect *Phys. Rev. Lett.* **53** 2173–6
[105] Polland H-J, Schultheis L, Kuhl J, Göbel E O and Tu C W 1985 Lifetime enhancement of two-dimensional excitons by the quantum-confined Stark effect *Phys. Rev. Lett.* **55** 2610
[106] Brus L E 1984 Electron–electron and electron-hole interactions in small semiconductor crystallites: the size dependence of the lowest excited electronic state *J. Chem. Phys.* **80** 4403–9
[107] Hiroshima T and Nishi K 1987 Quantum-confined stark effect in graded-gap quantum wells *J. Appl. Phys.* **62** 3360–5
[108] Ekinov A I, Efros A L, Shubina T V and Skvortsov A P 1990 Quantum-size stark effect in semiconductor microcrystals *J. Lumin.* **46** 97–100
[109] Empedocles S A and Bawendi M G 1997 Quantum-confined stark effect in single CdSe nanocrystallite quantum dots *Science* **278** 2114–7
[110] Seufert J, Obert M, Scheibner M, Gippius N A, Bacher G, Forchel A, Passow T, Leonardi K and Hommel D 2001 Stark effect and polarizability in a single CdSe/ZnSe quantum dot *Appl. Phys. Lett.* **79** 1033–5
[111] Rothenberg E, Kazes M, Shaviv E and Banin U 2005 Electric field induced switching of the fluorescence of single semiconductor quantum rods *Nano Lett.* **5** 1581–6
[112] Park K, Deutsch Z, Li J J, Oron D and Weiss S 2012 Single molecule quantum-confined Stark effect measurements of semiconductor nanoparticles at room temperature *ACS Nano* **6** 10013–23
[113] Marshall J D and Schnitzer M J 2013 Optical strategies for sensing neuronal voltage using quantum dots and other semiconductor nanocrystals *ACS Nano* **7** 4601–9
[114] Teitelboim A, Meir N, Kazes M and Oron D 2016 Colloidal double quantum dots *Acc. Chem. Res.* **49** 902–10
[115] Dias E A, Saari J I, Tyagi P and Kambhampati P 2012 Improving Optical gain performance in semiconductor quantum dots via coupled quantum shells *J. Phys. Chem.* C **116** 5407–13
[116] Dias E A, Sewall S L and Kambhampati P 2007 Light Harvesting and Carrier Transport in Core/Barrier/Shell Semiconductor Nanocrystals *J. Phys. Chem.* C **111** 708–13
[117] Dias E A, Grimes A F, English D S and Kambhampati P 2008 Single dot spectroscopy of two-color quantum dot/quantum shell nanostructures *J. Phys. Chem.* C **112** 14229–32
[118] Battaglia D, Blackman B and Peng X 2005 Coupled and decoupled dual quantum systems in one semiconductor nanocrystal *J. Am. Chem. Soc.* **127** 10889–97
[119] Soni U, Pal A, Singh S, Mittal M, Yadav S, Elangovan R and Sapra S 2014 Simultaneous type-I/type-II emission from CdSe/CdS/ZnSe nano-heterostructures *ACS Nano* **8** 113–23
[120] Teitelboim A and Oron D 2016 Broadband Near-Infrared to Visible Upconversion in Quantum Dot-Quantum Well Heterostructures *ACS Nano* **10** 446–52
[121] Zhao H, Sirigu G, Parisini A, Camellini A, Nicotra G, Rosei F, Morandi V, Zavelani-Rossi M and Vomiero A 2016 Dual emission in asymmetric 'giant' PbS/CdS/CdS core/shell/shell quantum dots *Nanoscale* **8** 4217–26
[122] Zhao H, Vomiero A and Rosei F 2015 Ultrasensitive, biocompatible, self-calibrating, multiparametric temperature sensors *Small* **11** 5741–6
[123] Razgoniaeva N, Yang M R, Colegrove C, Kholmicheva N, Moroz P, Eckard H, Vore A and Zamkov M 2017 Double-well colloidal nanocrystals featuring two-color photoluminescence *Chem. Mater.* **29** 7852–8
[124] Vlaskin V A, Janssen N, van Rijssel J, Beaulac R and Gamelin D R 2010 Tunable dual emission in doped semiconductor nanocrystals *Nano Lett.* **10** 3670–4
[125] McLaurin E J, Vlaskin V A and Gamelin D R 2011 Water-soluble dual-emitting nanocrystals for ratiometric optical thermometry *J. Am. Chem. Soc.* **133** 14978–80
[126] McLaurin E J, Fataftah M S and Gamelin D R 2013 One-step synthesis of alloyed dual-emitting semiconductor nanocrystals *Chem. Commun.* **49** 39–41
[127] Cao S, Zheng J J, Zhao J L, Yang Z B, Shang M H, Li C M, Yang W Y and Fang X S 2016 Robust and stable ratiometric temperature sensor based on Zn-In-S quantum dots with intrinsic dual-dopant ion emissions *Adv. Funct. Mater.* **26** 7224–33
[128] Lakowicz J R 2006 *Principles of fluorescence spectroscopy* 3 (New York: Springer) 9780387312781 (https://doi.org/10.1007/978-0-387-46312-4)
[129] Suzuki M, Husimi Y, Komatsu H, Suzuki K and Douglas K T 2008 Quantum dot FRET biosensors that respond to pH, to proteolytic or nucleolytic cleavage, to DNA synthesis, or to a multiplexing combination *J. Am. Chem. Soc.* **130** 5720–5
[130] Snee P T, Somers R C, Nair G, Zimmer J P, Bawendi M G and Nocera D G 2006 A ratiometric CdSe/ZnS nanocrystal pH sensor *J. Am. Chem. Soc.* **128** 13320–1
[131] Somers R C, Lanning R M, Snee P T, Greytak A B, Jain R K, Bawendi M G and Nocera D G 2012 A Nanocrystal-based ratiometric pH sensor for natural pH ranges *Chem. Sci.* **3** 2980–5
[132] Dennis A M, Rhee W J, Sotto D, Dublin S N and Bao G 2012 Quantum dot-fluorescent protein FRET probes for sensing intracellular pH *ACS Nano* **6** 2917–24
[133] Prasai D *et al* 2015 Electrical control of near-field energy transfer between quantum dots and two-dimensional semiconductors *Nano Lett.* **15** 4374–80
[134] Boeneman K, Mei B C, Dennis A M, Bao G, Deschamps J R, Mattoussi H and Medintz I L 2009 Sensing caspase 3 activity with quantum dot-fluorescent protein assemblies *J. Am. Chem. Soc.* **131** 3828–9
[135] Medintz I L, Clapp A R, Brunel F M, Tiefenbrunn T, Uyeda H T, Chang E L, Deschamps J R, Dawson P E and Mattoussi H 2006 Proteolytic activity monitored by fluorescence resonance energy transfer through quantum-dot-peptide conjugates *Nat. Mater.* **5** 581–9
[136] Algar W R, Malonoski A, Deschamps J R, Blanco-Canosa J B, Susumu K, Stewart M H, Johnson B J, Dawson P E and Medintz I L 2012 Proteolytic activity at quantum dot-conjugates: kinetic analysis reveals enhanced enzyme activity and localized interfacial 'hopping' *Nano Lett.* **12** 3793–802
[137] Diaz S A, Malonoski A P, Susumu K, Hofele R V, Oh E and Medintz I L 2015 Probing the kinetics of quantum dot-based proteolytic sensors *Anal. Bioanal. Chem.* **407** 7307–18
[138] Lowe S B, Dick J A, Cohen B E and Stevens M M 2012 Multiplex sensing of protease and kinase enzyme activity via orthogonal coupling of quantum dot-peptide conjugates *ACS Nano* **6** 851–7

[139] Wegner D K, Jin Z, Lindén S, Jennings T L and Hildebrandt N 2013 Quantum-Dot-based förster resonance energy transfer immunoassay for sensitive clinical diagnostics of low-volume serum samples *ACS Nano* **7** 7411-7419
[140] Kattke M D, Gao E J, Sapsford K E, Stephenson L D and Kumar A 2011 FRET-based quantum dot immunoassay for rapid and sensitive detection of Aspergillus amstelodami *Sensors* **11** 6396–410
[141] Clapp A R, Medintz I L, Fisher B R, Anderson G P and Mattoussi H 2005 Can luminescent quantum dots be efficient energy acceptors with organic dye donors? *J. Am. Chem. Soc.* **127** 1242–50
[142] Sapsford K E, Berti L and Medintz I L 2006 Materials for fluorescence resonance energy transfer analysis: beyond traditional donor-acceptor combinations *Angew. Chem., Int. Ed. Engl.* **45** 4562–89
[143] Medintz I and Hildebrandt N 2013 How to apply FRET: from experimental design to data *FRET- Förster Resonance Energy Transfer: From Theory to Applications* (Weinhein, Germany: Wiley-VCH) 59783527328161 (https://doi.org/10.1002/9783527656028.ch05)
[144] Degorce F, Card A, Soh S, Trinquet E, Knapik G P and Xie B 2009 HTRF: A technology tailored for drug discovery — a review of theoretical aspects and recent applications *Curr. Chem. Genomics* **3** 22–32
[145] Hildebrandt N, Charbonniere L J, Beck M, Ziessel R F and Lohmannsroben H G 2005 Quantum dots as efficient energy acceptors in a time-resolved fluoroimmunoassay *Angew. Chem., Int. Ed. Engl.* **44** 7612–5
[146] Wegner K D, Jin Z, Linden S, Jennings T L and Hildebrandt N 2013 Quantum-dot-based Forster resonance energy transfer immunoassay for sensitive clinical diagnostics of low-volume serum samples *ACS Nano* **7** 7411–9
[147] Wegner K D, Linden S, Jin Z, Jennings T L, el Khoulati R, Bergen en V, Henegouwen P M and Hildebrandt N 2014 Nanobodies and nanocrystals: highly sensitive quantum dot-based homogeneous FRET immunoassay for serum-based EGFR detection *Small* **10** 734–40
[148] Bhuckory S, Lefebvre O, Qiu X, Wegner K D and Hildebrandt N 2016 Evaluating Quantum Dot performance in homogeneous FRET Immunoassays for prostate specific antigen *Sensors* **16** 197
[149] Mattera L *et al* 2016 Compact quantum dot-antibody conjugates for FRET immunoassays with subnanomolar detection limits *Nanoscale* **8** 11275–83
[150] Dennis A M, Sotto D C, Mei B C, Medintz I L, Mattoussi H and Bao G 2010 Surface ligand effects on metal-affinity coordination to quantum dots: implications for nanoprobe self-assembly *Bioconjug. Chem.* **21** 1160–70
[151] Zhang Y, Zhang H, Hollins J, Webb M E and Zhou D 2011 Small-molecule ligands strongly affect the Forster resonance energy transfer between a quantum dot and a fluorescent protein *Phys. Chem. Chem. Phys.* **13** 19427–36
[152] Susumu K *et al* 2011 Multifunctional compact zwitterionic ligands for preparing robust biocompatible semiconductor quantum dots and gold nanoparticles *J. Am. Chem. Soc.* **133** 9480–96
[153] Uyeda H T, Medintz I L, Jaiswal J K, Simon S M and Mattoussi H 2005 Synthesis of compact multidentate ligands to prepare stable hydrophilic quantum dot fluorophores *J. Am. Chem. Soc.* **127** 3870–8
[154] Ma L, Tu C, Le P, Chitoor S, Lim S J, Zahid M U, Teng K W, Ge P, Selvin P R and Smith A M 2016 Multidentate polymer coatings for compact and homogeneous quantum dots with efficient bioconjugation *J. Am. Chem. Soc.* **138** 3382–94
[155] Bhuckory S, Mattera L, Wegner K D, Qiu X, Wu Y T, Charbonnière L J, Reiss P and Hildebrandt N 2016 Direct conjugation of antibodies to the ZnS shell of quantum dots for FRET immunoassays with low picomolar detection limits *Chemical Communications* **52** 14423–5
[156] Qiu X, Wegner K D, Wu Y T, Henegouwen P M P V B E, Jennings T L and Hildebrandt N 2016 Nanobodies and antibodies for duplexed EGFR/HER2 immunoassays using terbium-to-quantum dot FRET *Chem. Mater.* **28** 8256–67
[157] Geißler D, Stufler S, Lohmannsroben H G and Hildebrandt N 2013 Six-color time-resolved forster resonance energy transfer for ultrasensitive multiplexed biosensing *J. Am. Chem. Soc.* **135** 1102–9
[158] Gnach A and Bednarkiewicz A 2012 Lanthanide-doped up-converting nanoparticles: merits and challenges *Nano. Today* **7** 532–63
[159] Doughan S, Uddayasankar U and Krull U J 2015 A paper-based resonance energy transfer nucleic acid hybridization assay using upconversion nanoparticles as donors and quantum dots as acceptors *Anal. Chim. Acta.* **878** 1–8
[160] Mattsson L, Wegner K D, Hildebrandt N and Soukka T 2015 Upconverting nanoparticle to quantum dot FRET for homogeneous double-nano biosensors *RSC Adv.* **5** 13270–7
[161] Pons T, Medintz I L, Wang X, English D S and Mattoussi H 2006 Solution-phase single quantum dot fluorescence resonance energy transfer *J. Am. Chem. Soc.* **128** 15324–31
[162] Uddayasankar U, Zhang Z, Shergill R T, Gradinaru c.c. and Krull U J 2014 Isolation of monovalent quantum dot-nucleic acid conjugates using magnetic beads *Bioconjug. Chem.* **25** 1342–50
[163] Farlow J, Seo D, Broaders K E, Taylor M J, Gartner Z J and Jun Y W 2013 Formation of targeted monovalent quantum dots by steric exclusion *Nat. Methods* **10** 1203–5
[164] Wang G, Li Z and Ma N 2018 Next-generation dna-functionalized quantum dots as biological sensors *ACS Chem Biol* **13** 1705–13
[165] Tikhomirov G, Hoogland S, Lee P E, Fischer A, Sargent E H and Kelley S O 2011 DNA-based programming of quantum dot valency, self-assembly and luminescence *Nat. Nanotechnol.* **6** 485–90
[166] Coopersmith K, Han H and Maye M M 2015 Stepwise assembly and characterization of DNA linked two-color quantum Dot clusters *Langmuir* **31** 7463–71
[167] Altıntas Y, Talpur M Y and Mutlugün E 2017 Efficient förster resonance energy transfer donors of In(Zn)P/ZnS Quantum dots *J. Phys. Chem.* C **121** 3034–43
[168] Bissell R A, de Silva A P, Gunaratne H Q N, Lynch P L M, Maguire G E M and Sandanayake K R A S 1992 Molecular fluorescent signalling with 'fluor–spacer–receptor' systems: approaches to sensing and switching devices via supramolecular photophysics *Chem. Soc. Rev.* **21** 187–95
[169] Daly B, Ling J and de Silva A P 2015 Current developments in fluorescent PET (photoinduced electron transfer) sensors and switches *Chem. Soc. Rev.* **44** 4203–11
[170] Tvrdy K, Frantsuzov P A and Kamat P V 2011 Photoinduced electron transfer from semiconductor quantum dots to metal oxide nanoparticles *Proc. Natl Acad. Sci.* **108** 29–34
[171] Zhu H, Yang Y, Wu K and Lian T 2016 Charge transfer dynamics from photoexcited semiconductor quantum dots *Annu. Rev. Phys. Chem.* **67** 259–81
[172] Gauci L A, Kelland L G and Magri D C 2013 Luminescent 'On-Off' CdSe/ZnS quantum dot chemodosimeter for hydroxide based on photoinduced electron transfer from a carboxylate moiety *J. Fluoresc.* **23** 793–8
[173] Dhenadhayalan N, Lee H L, Yadav K, Lin K C, Lin Y T and Chang A H 2016 Silicon Quantum Dot-Based Fluorescence Turn-On Metal Ion Sensors in Live Cells *ACS Appl. Mater. Interfaces* **8** 23953–62
[174] Kaur N, Singh N, McCaughan B and Callan J F 2010 AND molecular logic using semiconductor quantum dots *Sens. Actuators B Chem.* **144** 88–91
[175] de Silva A P, Moody T S and Wright G D 2009 Fluorescent PET (photoinduced electron transfer) sensors as potent analytical tools *Analyst* **134** 2385–93
[176] Mulrooney R C, Singh N, Kaur N and Callan J F 2009 An 'off-on' sensor for fluoride using luminescent CdSe/ZnS quantum dots *Chem. Commun.* 686–8

[177] Nag O K *et al* 2017 Quantum Dot-Peptide-fullerene bioconjugates for visualization of *in Vitro* and *in Vivo* cellular membrane potential *ACS Nano* **11** 5598–613
[178] Yun C S, Javier A, Jennings T, Fisher M, Hira S, Peterson S, Hopkins B, Reich N O and Strouse G F 2005 Nanometal surface energy transfer in optical rulers, breaking the FRET barrier *J. Am. Chem. Soc.* **127** 3115–9
[179] Breshike C J, Riskowski R A and Strouse G F 2013 Leaving forster resonance energy transfer behind: nanometal surface energy transfer predicts the size-enhanced energy coupling between a metal nanoparticle and an emitting dipole *J. Phys. Chem.* C **117** 23942–9
[180] Jennings T L, Singh M P and Strouse G F 2006 Fluorescent lifetime quenching near d = 1.5 nm gold nanoparticles: probing NSET validity *J. Am. Chem. Soc.* **128** 5462–7
[181] Chen C, Midelet C, Bhuckory S, Hildebrandt N and Werts M H V 2018 Nanosurface Energy transfer from long-lifetime terbium donors to gold nanoparticles *The Journal of Physical Chemistry* C **122** 17566–74
[182] Li M, Wang Q, Shi X, Hornak L A and Wu N 2011 Detection of mercury(II) by quantum dot/DNA/gold nanoparticle ensemble based nanosensor via nanometal surface energy transfer *Anal. Chem.* **83** 7061–5
[183] Kikkeri R, Padler-Karavani V, Diaz S, Verhagen A, Yu H, Cao H, Langereis M A, De Groot R J, Chen X and Varki A 2013 Quantum dot nanometal surface energy transfer based biosensing of sialic acid compositions and linkages in biological samples *Anal. Chem.* **85** 3864–70
[184] Huang D, Niu C, Wang X, Lv X and Zeng G 2013 'Turn-on' fluorescent sensor for Hg^{2+} based on single-stranded DNA functionalized Mn:CdS/ZnS quantum dots and gold nanoparticles by time-gated mode *Anal. Chem.* **85** 1164–70
[185] Choi Y, Cho Y, Kim M, Grailhe R and Song R 2012 Fluorogenic quantum dot-gold nanoparticle assembly for beta secretase inhibitor screening in live cell *Anal. Chem.* **84** 8595–601
[186] Pons T, Medintz I L, Sapsford K E, Higashiya S, Grimes A F, English D S and Mattoussi H 2007 On the quenching of semiconductor quantum dot photoluminescence by proximal gold nanoparticles *Nano Lett.* **7** 3157–64
[187] Chang E, Miller J S, Sun J, Yu W W, Colvin V L, Drezek R and West J L 2005 Protease-activated quantum dot probes *Biochem. Biophys. Res. Commun.* **334** 1317–21
[188] Griffin J, Singh A K, Senapati D, Rhodes P, Mitchell K, Robinson B, Yu E and Ray P C 2009 Size- and distance-dependent nanoparticle surface-energy transfer (NSET) method for selective sensing of hepatitis C virus RNA *Chem. Eur. J.* **15** 342–51
[189] Samanta A, Zhou Y, Zou S, Yan H and Liu Y 2014 Fluorescence quenching of quantum dots by gold nanoparticles: a potential long range spectroscopic ruler *Nano Lett.* **14** 5052–7
[190] Han H, Valle V and Maye M M 2012 Probing Resonance Energy Transfer and Inner Filter Effects in Quantum Dot-Large Metal Nanoparticle Clusters using a DNA-Mediated Quench and Release Mechanism *J. Phys. Chem.* C **116** 22996–3003
[191] Uddayasankar U and Krull U J 2015 Energy transfer assays using quantum dot-gold nanoparticle complexes: optimizing oligonucleotide assay configuration using monovalently conjugated quantum dots *Langmuir* **31** 8194–204
[192] Brazhnik K, Sokolova Z, Baryshnikova M, Bilan R, Efimov A, Nabiev I and Sukhanova A 2015 Quantum dot-based lab-on-a-bead system for multiplexed detection of free and total prostate-specific antigens in clinical human serum samples *Nanomedicine* **11** 1065–75
[193] Wu M, Massey M, Petryayeva E and Algar W R 2015 Energy transfer pathways in a quantum dot-based concentric FRET configuration *J. Phys. Chem.* C **119** 26183–95
[194] Chen C *et al* 2018 Single-nanoparticle cell barcoding by tunable FRET from lanthanides to quantum dots *Angew. Chem., Int. Ed. Engl.* **57** 13686–90
[195] Yong K T, Law W C, Hu R, Ye L, Liu L, Swihart M T and Prasad P N 2013 Nanotoxicity assessment of quantum dots: from cellular to primate studies *Chem. Soc. Rev.* **42** 1236–50
[196] Wu T, Zhang T, Chen Y and Tang M 2016 Research advances on potential neurotoxicity of quantum dots *J. Appl. Toxicol.* **36** 345–51
[197] Wu T and Tang M 2014 Toxicity of quantum dots on respiratory system *Inhal. Toxicol.* **26** 128–39
[198] van der Stam W, Berends A C, de M and Donega C 2016 Prospects of Colloidal Copper Chalcogenide Nanocrystals *Chemphyschem* **17** 559–81
[199] Das A and Snee P T 2016 Synthetic developments of nontoxic quantum dots **17** 598–617
[200] Xu G, Zeng S, Zhang B, Swihart M T, Yong K T and Prasad P N 2016 New generation cadmium-free quantum dots for biophotonics and nanomedicine *Chem. Rev.* **116** 12234–327
[201] Tamang S, Lincheneau C, Hermans Y, Jeong S and Reiss P 2016 Chemistry of InP nanocrystal syntheses *Chem. Mater.* **28** 2491–506
[202] Speranskaya E S, Beloglazova N V, Abe S, Aubert T, Smet P F, Poelman D, Goryacheva I Y, De Saeger S and Hens Z 2014 Hydrophilic, bright $CuInS_2$ quantum dots as Cd-free fluorescent labels in quantitative immunoassay *Langmuir* **30** 7567–75
[203] Ulep T H and Yoon J Y 2018 Challenges in paper-based fluorogenic optical sensing with smartphones *Nano. Converg.* **5** 14
[204] Aubin-Tam M E and Hamad-Schifferli K 2008 Structure and function of nanoparticle-protein conjugates *Biomed. Mater.* **3** 034001
[205] Sapsford K E, Algar W R, Berti L, Gemmill K B, Casey B J, Oh E, Stewart M H and Medintz I L 2013 Functionalizing nanoparticles with biological molecules: developing chemistries that facilitate nanotechnology *Chem. Rev.* **113** 1904–2074
[206] Hildebrandt N 2011 Biofunctional quantum dots: controlled conjugation for multiplexed biosensors *ACS Nano* **5** 5286–90
[207] Zhou W, Huang P J, Ding J and Liu J 2014 Aptamer-based biosensors for biomedical diagnostics *Analyst* **139** 2627–40
[208] Chen Y, Thakar R and Snee P T 2008 Imparting nanoparticle function with size-controlled amphiphilic polymers *J. Am. Chem. Soc.* **130** 3744–5
[209] Jennings T L *et al* 2011 Reactive semiconductor nanocrystals for chemoselective biolabeling and multiplexed analysis *ACS Nano* **5** 5579–93
[210] Jung J, Solanki A, Memoli K A, Kamei K, Kim H, Drahl M A, Williams L J, Tseng H R and Lee K 2010 Selective inhibition of human brain tumor cells through multifunctional quantum-dot-based siRNA delivery *Angew. Chem., Int. Ed. Engl.* **49** 103–7
[211] Singh N, Agrawal A, Leung A K, Sharp P A and Bhatia S N 2010 Effect of nanoparticle conjugation on gene silencing by RNA interference *J. Am. Chem. Soc.* **132** 8241–3
[212] Bosch P J, Correa I R Jr, Sonntag M H, Ibach J, Brunsveld L, Kanger J S and Subramaniam V 2014 Evaluation of fluorophores to label SNAP-tag fused proteins for multicolor single-molecule tracking microscopy in live cells *Biophys. J.* **107** 803–14
[213] Ohyanagi T, Shima T, Okada Y, Tsukasaki Y, Komatsuzaki A, Tsuboi S and Jin T 2015 Compact and stable SNAP ligand-conjugated quantum dots as a fluorescent probe for single-molecule imaging of dynein motor protein *Chem. Commun.* **51** 14836–9
[214] Komatsuzaki A, Ohyanagi T, Tsukasaki Y, Miyanaga Y, Ueda M and Jin T 2015 Compact halo-ligand-conjugated quantum dots for multicolored single-molecule imaging of overcrowding GPCR proteins on cell membranes *Small* **11** 1396–401

[215] So M K, Yao H and Rao J 2008 HaloTag protein-mediated specific labeling of living cells with quantum dots *Biochem. Biophys. Res. Commun.* **374** 419–23
[216] Liu D S, Phipps W S, Loh K H, Howarth M and Ting A Y 2012 Quantum dot targeting with lipoic acid ligase and HaloTag for single-molecule imaging on living cells *ACS Nano* **6** 11080–7
[217] Zhang H, Feng G, Guo Y and Zhou D 2013 Robust and specific ratiometric biosensing using a copper-free clicked quantum dot-DNA aptamer sensor *Nanoscale* **5** 10307–15
[218] Chen Y *et al* 2018 A Ligand System for the Flexible Functionalization of Quantum Dots via Click Chemistry *Angew. Chem., Int. Ed. Engl.* **57** 4652–6